$/N$-39

68728

$p.54$

Differential Continuum Damage Mechanics Models for Creep and Fatigue of Unidirectional Metal Matrix Composites

S.M. Arnold
Lewis Research Center
Cleveland, Ohio

and

S. Kruch
Office National D'Etudes et de Recherches Aerospatiales
Chatillon, France

NASA

DIFFERENTIAL CONTINUUM DAMAGE MECHANICS MODELS FOR CREEP AND FATIGUE OF UNIDIRECTIONAL METAL MATRIX COMPOSITES

By

S. M. Arnold
National Aeronautics and Space Administration
Lewis Research Center
Cleveland Ohio, 44135.

and

S. Kruch
Office National d' Etudes et de Recherches Aerospatiales
92322 Chatillon, France.

ABSTRACT

Three multiaxial isothermal continuum damage mechanics model for creep, fatigue, and creep/fatigue interaction of a unidirectional metal matrix composite volume element are presented, only one of which will be discussed in depth. Each model is phenomenological and stress based, with varying degrees of complexity to accurately predict the initiation and propagation of intergranular and transgranular defects over a wide range of loading conditions. The development of these models are founded on the definition of an initially transversely isotropic fatigue limit surface, static fracture surface, normalized stress amplitude function and isochronous creep damage failure surface, from which both fatigue and creep damage evolutionary laws can be obtained. The anisotropy of each model is defined through physically meaningful invariants reflecting the local stress and material orientation. All three transversely isotropic models have been shown, when taken to their isotropic limit, to directly simplify to previously developed and validated creep and fatigue continuum damage theories.

Results of a nondimensional parametric study illustrate i) the flexibility of the present formulation when attempting to characterize a large class of composite materials and ii) its ability to predict anticipated qualitative trends in the fatigue behavior of unidirectional metal matrix composites. Additionally, the potential for the inclusion of various micromechanical effects (e.g. fiber/matrix bond strength, fiber volume fraction, etc.), into the phenomenological anisotropic parameters are noted, as well as a detailed discussion regarding the necessary exploratory and characterization experiments needed to utilize the featured damage theories.

1.0 INTRODUCTION

In recent years, due to advances in scanning electron microscopy, acoustic emission techniques as well as other nondestructive testing methods, a consensus has emerged that the nonlinear response of solids and ultimately their mechanical strength are dependent not only on the basic structure of the material but also on the type, distribution, size and orientation of the defects in its structure. As a result a

relatively new branch of continuum mechanics, known as Continuum Damage Mechanics (CDM), has emerged. Like Continuum Mechanics, which allows one to describe (over an appropriate representative volume element) the heterogeneous microprocesses involved during the straining of materials and structures at the macroscale; CDM allows one to describe the material's progressive deterioration (damage) from the virgin state (no damage) to the final state, corresponding generally to macro–crack initiation (or the "breaking up" of the representative volume element). Therefore, CDM allows one to predict the life limiting macroscopic properties such as rupture strength, fatigue life, or creep rupture lifetime of the material.

The tracking, or description, of the evolution of damage is accomplished through the introduction of special thermodynamic (internal) field variables representing in an appropriate statistical sense, the distribution and density of defects locally. Numerous damage theories, both micromechanical [1–6][1] and phenomenological [7–11], for example, have been proposed and discussed in the literature. The reason behind such diversity in the mathematical nature of the damage variable(s) (e.g., scalar [7,12,13], vectors [14,15] and tensors [12,16,17]) and thus the damage theories, stems from the difficulty associated with directly measuring "damage" macroscopically and the degree of approximation with which the internal variables describe the salient aspects of the macroscopic effects of the micro–defect kinematics. For a number of excellent review articles and books on this subject the reader is referred to references [7,12,18–24].

In this paper a CDM isothermal transversely isotropic creep, fatigue, and creep/fatigue model, with a *scalar* damage internal variable, oriented toward unidirectional metallic composites, will be described. These models are extensions of previously developed and validated models, developed at ONERA (Office Nationale d'Etudes et de Recherches Aerospatiales), [10,11,18,19,25,26,27,28] for isotropic monolithic metals. As a result, the paper begins with a brief review of CDM in general, and in particular, the work undertaken by Chaboche and his colleagues at ONERA, so as to provide a foundation to describe the extension of the ONERA models to transversely isotropic materials (e.g., metal matrix composites). Subsequent to the multiaxial statement of the transversely isotropic CDM models, a nondimensional uniaxial parametric study is undertaken to illustrate the various features and flexibilities of the proposed extensions. The paper then concludes with a

---

[1]Square brackets, i.e. [ ], will indicate suggested references for further reading.

discussion regarding exploratory and characterization experiments required to utilize and validate the proposed forms.

2.0 MEASURES AND DEFINITIONS OF DAMAGE

Material (lattice) defects can be roughly classified with respect to their geometry into i) point defects; for example vacancies, interstitial and impurity atoms, ii) line defects (dislocations), iii) plane defects (slip planes and cracks), and iv) volume defects (cavities and inclusions). Numerous ways are available to define the internal variables associated with these defects and damage processes. Each definition, however, must correspond to some method of measurement and implies a given approach, either a micromechanical or phenomenological one. Here, four typical approaches will be briefly stated.

Measurements at the microstructural scale (i.e., density of micro–cracks in fatigue or the volume fraction of cavities in ductile damage) lead to microscopic models that can be integrated over the macroscopic volume element to obtain the properties of the damaged volume element. However, difficulty is encountered when incorporating these results into life prediction methods.

Measurements of macro physical parameters (such as density, acoustic emission and resistivity) may lead to some consistent macroscopic definitions of damage parameters but require the definition of a global model to convert them into properties which characterize mechanical resistance.

Measures of remaining life are used to account for the cumulative aspects of damage processes in the life prediction methods but do not directly lead to a damage constitutive law. They do however, provide insight into interesting properties of damage, for example in fatigue they indicate that the damage evolution equations must be non–separable relative to the damage and loading variables [29].

Measurements of variations in the macro mechanical behavior (i.e., modification of elastic, plastic or viscoplastic properties) are the most appropriate from a phenomenological point of view. These measurements are easier to interpret in terms of damage variables using the concept of effective stress [12,28] with an

3

equivalence in strain, Fig. 1. This is the approach that will be followed throughout the remainder of this report.

The effective stress $(\bar{\sigma})$ concept, with an equivalence in strain as put forth by Lemaitre and Chaboche [12] states that a damaged volume of material under the applied stress (σ) shows the same strain response (whether the behavior is elastic, plastic, or viscoplastic) as the undamaged one submitted to the effective stress $(\bar{\sigma})$. In mathematical form

$$\bar{\sigma} = \frac{A}{\tilde{A}} \; \sigma = \frac{\sigma}{1-D} \tag{1}$$

where $\tilde{A} = A-A_D$ and the damage D represents the loss of effective area (A_D/A) taking into account decohesions and local stress concentrations. This definition has been supported by the results of homogenization techniques [30] and damage measures utilizing this concept have been demonstrated under various situations, for example, in the case of ductile rupture [31], creep damage [32], and fatigue damage for both monolithic and composite materials [18,33,34].

3.0 CDM MODELS FOR INITIALLY ISOTROPIC MATERIALS

Different damage variables are associated with different damage processes, such as creep, fatigue, ductile and brittle damage, and have been discussed in the literature extensively as noted above. Here we will confine ourselves to the modeling of creep, fatigue and creep/fatigue damage using a scalar damage measure in monolithic metals and then extend this discussion, in subsequent sections, to metal matrix composites by allowing the anisotropic evolution of this measure. Figure 2 clearly illustrates the damage mechanisms for the three cases of interest, i.e., creep, fatigue and creep/fatigue interaction.

3.1 Creep Damage

In Fig. 2a the two primary damage mechanisms [35,36], nucleation and growth of intergranular defects (typically by a diffusion process) are illustrated schematically when the material is subjected to a pure creep loading condition. Recently, Hayhurst [37] has shown that it is possible to make some connection between the equations

4

obtained from a materials science approach and the more macroscopic ones developed under the framework of CDM.

CDM was first developed for the case of creep damage by Kachanov [38] and, Rabotnov [23], since then the concept of effective stress has been shown to predict tertiary creep curves as well as changes in creep ductility [39]. Leckie and Hayhurst [8,13,40,41] have generalized the classical [23,38] uniaxial creep damage equations to multiaxial stress conditions by describing isodamage surfaces (or isochronous surfaces) defined in terms of three stress invariants i) the octahedral shear stress $\bar{J}_2(\sigma)$, which is related to the effects of shear, ii) the hydrostatic stress $\mathcal{J}_1(\sigma)$, which greatly affects the growth of cavities; and iii) the maximum principal stress $J_0(\sigma) = \sigma_{max}$, which opens the micro-cracks and causes them to grow. The equivalent stress is then defined through a linear combination of these invariants :

$$\chi(\sigma) = \alpha_c \, J_0(\sigma) + \beta_c \mathcal{J}_1(\sigma) + (1-\alpha_c-\beta_c) \, \bar{J}_2(\sigma) \qquad (2)$$

here α_c and β_c are coefficients dependent upon the material. The form of the resulting creep damage model is given in Table I. Note that here the exponent k is taken to be a constant, thus implying linear accumulation of creep damage even though the evolution of damage may be nonlinear.

Furthermore, the results of creep-like cyclic tests (e.g., high frequency-low amplitude or high amplitude-low frequency) have shown the need to include some factor relating the response time of the material versus that of the rate of loading. For example, when a material is subjected to a high frequency loading with a mean stress equal to zero, the material damage induced by creep is negligible, thereby leading to the case of "pure" fatigue damage. However, when the material is subjected to a high frequency and a low or medium amplitude with a high mean stress, the damage induced by creep is dominant. Therefore a new material parameter (τ) and a "delayed" stress (σ^d_{ij}) were introduced into the formulation, so as to account for the lag time between load application and material response [26]. As a result, given a high frequency load history, the delayed stress is equal to the mean stress while for a low frequency load history the delayed stress is the real (or applied) stress.

3.2 Fatigue Damage

In Fig. 2b, the fatigue crack initiation and growth process is illustrated schematically, with the damage (D) being associated , macroscopically, with the initiation and propagation of transgranular defects (e.g., slip bands and micro-cracks). For example the micro-crack measurements made by Cailletaud and Levaillant [42], Hua and Socie [43], and Socie et. al. [44], have shown the possible equivalence between the definition of D by the effective stress concept, the definition of D in terms of the remaining life concept, and the quantification of physical damage in terms of micro-cracking. A number of fatigue damage models have been proposed in the past [12,18,21]. A general form, depending upon one's choice for α (the exponent which may also be a function of stress), as indicated by Chaudonneret and Chaboche [45], that leads to rules considered earlier by various authors [10,25,26,46,47,48] is given by:

$$dD = D^{\alpha(\sigma_m, \bar{\sigma})} \left[\frac{\sigma_m - \bar{\sigma}}{M(\bar{\sigma})} \right]^{\beta} dN \qquad (3)$$

where σ_m and $\bar{\sigma}$ are, respectively, the maximum and mean stress within a cycle N.

In the case of fatigue, several aspects need to be considered when developing a phenomenological model:

a)   the existence of micro-initiation and micro-propagation stages,

b)   the existence of a fatigue or endurance limit and its marked decrease after prior damage,

c)   the existence of a static limit (ultimate stress level),

d)   the effect of mean-stress on the fatigue limit or the S-N curves themselves, and

e)   the typical nonlinear-cumulative effects for two level tests or block-program loading conditions.

Three CDM fatigue models, developed at ONERA, which to varying degrees accurately predict the above observations, are given in multiaxial form in Table II and uniaxial form in Table III. Note that these models are obtained from equation (3) (predominantly developed from a remaining life concept) and

6

incorporated into a CDM model utilizing the effective stress concept, by a convenient change of variable (i.e., D*), that is :

$$D = 1 - (1 - D^*)^{1+\beta} \qquad (4)$$

The ability of equation (3), and therefore those fatigue models in Table II and III, to represent the required nonlinear accumulation during a two level or block–program loading test is directly linked to the dependency of α on σ_m and $\bar{\sigma}$; thus rendering the equations non–separable. It is this nonseparability and not the nonlinearity of the damage evolution equation that permits the modeling of a nonlinear accumulation of damage [29]. Model I, was proposed in 1974 [49] and has since been exercised for a number of different applications and materials [50–52]. Results indicate good predictive capabilities under varying fatigue cycles, even though a single scalar state variable D represents both micro–initiation and micro–propagation periods. However, due to this lack of separation, a deficiency in Model I was observed when analyzing fatigue loading histories with prior creep or creep like (e.g., high cycle, low amplitude fatigue cycles) loading histories. Furthermore microstructural observations have indicated that fatigue damage can be divided into two periods, [53,54] the initiation period (corresponding to the creation of micro–cracks) and the propagation period (which is characterized by the inward growth in the material of a few micro–cracks).

Therefore in Model II a separation between the micro–crack initiation and propagation stages was introduced. Note that in Model II, α is assumed to be constant, thereby producing only linear damage accumulation (Miner's rule) during the propagation stage. This does not, however, imply that the damage D (i.e., D = $D_{initiation}$ + $D_{propagation}$) is restricted to only linear accumulation, as the damage accumulation can be shifted by an increase or decrease in the number of cycles for crack initiation. As a result model II can be shown to give the Manson Double Linear Damage Rule (OLDR). Additionally, in model II, the initiation of microcracks are influenced by the frequency (ν) of the applied loading due to the fact that differences in the experimental results were observed when varying the frequency of loading, particularly when at low frequency (e.g., $0 < \nu < 10$ Hz) levels.

Model III has been recently suggested as a compromise between Models I and II, in that it has the simplicity of Model I (no separation between initiation and

propagation is assumed) yet gives rise to a non evanescent fatigue limit by the introduction of a term representing the fatigue limit of propagation $(\sigma_{\ell p})$.

3.3 Creep–Fatigue Interaction

In Fig. 2c the interaction of intergranular and transgranular defects is depicted schematically. It is surmised, within the pertinent domain where creep–fatigue interaction is applicable, that the presence of cavities allow for easier crack propagation and that the increase in stress intensity at a crack tip causes an increase in the nucleation and coalescence of voids.

Analytically this interaction is represented using the effective stress concept, by assuming that the *mechanical effects* of creep and fatigue damage can be directly added, i.e.,

$$
\begin{aligned}
dD &= dD_C + dD_F \\
&= f_C(\sigma,T,D,...) \; dt + f_F(\sigma_m,\bar{\sigma},T,D,...) \; dN
\end{aligned}
\tag{5}
$$

where f_C and f_F represent the characteristic functions of creep and fatigue respectively as described above and $D = D_C + D_F$. Thus the two functions (f_C and f_F) can be determined independently from pure tensile creep tests and pure high frequency fatigue tests. The conditions under which accumulation of both macroscopic effects would take place (e.g., low frequency or loadings with hold times) are then predicted by integrating numerically the above equations. This approach has been shown to give reasonable results for several materials [12,49,50].

It is primarily in this context (creep/fatigue interaction) that the main distinctions between models I, II and III of Table II can be observed. For example utilizing the creep model of Table I (as will be the case henceforth) and the fatigue model I or III of Table II for the functions f_C and f_F, respectively, one can immediately see that interaction between the two damage measures occurs from the outset. However if the function f_F is comprised of Model II, interaction between creep and fatigue damage measures does not occur until crack initiation has occurred.

4.0 CDM MODELS FOR INITIALLY ANISOTROPIC MATERIALS

The Continuum Damage Mechanics approach, which supports the above described global measure of fatigue damage in monolithic isotropic materials, presents

two deficiencies which are inconsistent with a continuum approach. They are, i) the surface character of fatigue damage and ii) the fact that during the propagation stage the number of large defects is small. Interestingly enough, however, these deficiencies do not appear to have diminished the correct description of many experimental results in terms of cumulative fatigue damage.

It is the authors contention that these two theoretical deficiencies will be removed when one establishes a representative volume element (RVE) on the mesostructural scale of a composite material; since now the surface character of fatigue will transcend to the interface region of each constituent (or phase) and the number of large defects occurring during the propagation period will similarly increase. This hypothesis is borne out by experimental observation [55,56] under specific thermal and mechanical loading histories. Although, there are a number of surface and environmental effects which will not necessarily transcend to the fibers, for example those effects which are associated with oxidation in the SiC/Ti 15–3 system [57]. A nonrigorous definition of an RVE for a given composite material is given in Fig. 3 and in short insists upon the inclusion of a sufficient number of unit cells within the RVE to allow (statistically) the homogenization of the heterogeneous nature of the material.

Figure 4 depicts, the extension of the previously described creep, fatigue and creep/fatigue damage mechanisms of Fig. 2 to the mesostructural scale, in which the surface or interface of a constituent (the fiber) plays the role (on the mesostructural scale) of a grain (and therefore grain boundary) on the microscopic scale. Here similar damage mechanisms are postulated to occur on the mesostructural scale as those on the microstructural scale, and due to the internal structure of the material, a sufficient number of defects will be present to allow a theoretically consistent continuum representation of creep and fatigue damage.

In addition to the matrix cracking and formation of micro–cracks around the fibers, other damage modes must be included such as fiber breaking, fiber/matrix debonding and interlaminar cracks. It has been noted that damage occurs in the form of different multiple cracking modes and that there is no isolated single crack that dominates the development of damage. Similarly in composite laminates damage develops along preferred orientations, for example, matrix cracks in off axis plies typically are channeled by the fibers in those plies and interlaminar planar cracks grow along fibers in the neighboring plies [58].

These direction oriented damage modes suggest the need for some direction dependent damage variable (e.g., a vector or tensor representation). It is assumed in

the present work that the damage measure is a <u>scalar</u> but that the damage evolution is anisotropic. This is believed to be justified based on the strong initial anisotropy of the composite. Furthermore, as discussed earlier the definition of effective stress and the concept of remaining life will be utilized to measure and interpret damage.

4.1 Transversely Isotropic Creep Damage

Figure 4a is the mesostructural counter part to Fig. 2a and recently Robinson et al. [59] extended the creep damage model proposed by Leckie [40,41] and Leckie and Hayhurst [8,13] to metallic composites. This extension was accomplished by introducing into the isochronous damage function appropriate stress invariants that correspond to the local maximum transverse tension (stress normal to the local fiber direction) and longitudinal shear (shear stress on planes containing the fibers and in a direction along the fibers) within a unidirectional metallic composite. These invariants are included based on the anticipation that the associated stress may strongly influence void growth at the fiber–matrix interface (as this interface is postulated to play a role, on the mesostructural scale, analogous to that of grain boundaries on the microstructural scale and interfacial degradation); and, consequently may correlate with a creep rupture mechanism based on interfacial degradation through diffusion related void growth [56,60].

The physically meaningful invariants I_1, I_2 and I_3, representing the maximum transverse shear stress, longitudinal shear stress and the maximum normal stress in the fiber direction, respectively, are defined as (cf. [61,62]);

$$I_1 = J_2 - \hat{I} + \frac{1}{4} I_3$$

$$I_2 = \hat{I} - I_3 \tag{6}$$

$$I_3 = I^2$$

in which

$$J_2 = \frac{1}{2} S_{ij} S_{ij}$$

$$I = D_{ij} S_{ij}$$

$$\hat{I} = D_{ij} S_{jk} S_{ki}$$

$$D_{ij} = d_i d_j$$

$$S_{ij} = \sigma_{ij} - \frac{1}{3} \sigma_{kk} \delta_{ij}$$

and d_i (i=1,2,3) are the components of a unit vector denoting the local fiber direction. An additional invariant is required for the present formulation (i.e., the maximum transverse tensile stress) and is given in [59] as:

$$\mathcal{N} = < \frac{1}{2} (\mathcal{A}_1 - \mathcal{A}_2) + S > \qquad (7)$$

where :

$$< f > \begin{cases} = 0 \text{ if } f < 0 \\ = f \text{ if } f \geq 0 \end{cases}$$

$$\mathcal{A}_1 = \sigma_{ii}$$

$$\mathcal{A}_2 = D_{ij} \sigma_{ji}$$

$$S = \sqrt{I_1}$$

Thus the isochronous failure surface (Δ) is assumed [59] to be a linear function of the two invariants $\mathcal{N}$ and $\mathcal{S}$, i.e.,

$$\Delta = \frac{1}{\sigma_0} (\mathcal{N} + \alpha_c \mathcal{S}) \qquad (8)$$

where :

$$\mathscr{S} = \sqrt{I_2}$$

in which α_c is a material constant and σ_0 is a normalizing reference stress. An alternative isochronous failure surface (Δ), assumed here, can be written as;

$$\Delta = \frac{1}{\sigma_0} (\beta_c \mathscr{I}_1 + 3(1-\alpha_c-\beta_c) S + \alpha_c \mathscr{S})$$ (9)

in which the hydrostatic state of stress, maximum transverse shear and longitudinal shear stress are assumed to be the dominant damage measures. Note that the two isochronous surfaces defined in equations (8) and (9) are similar, provided β_c is taken to be zero, since S is related to the maximum transverse stress $\mathscr{N}$ (cf. eq.(7)), i.e.,

$$S = \{\mathscr{N} - \frac{1}{2} (\mathscr{I}_1 - \mathscr{I}_2)\}$$

The specific functional form for Δ must be determined experimentally as discussed by Robinson et. al. [59] and Leckie [40,41].

The damage evolutionary law [8,40], extended now (through the isochronous failure surface) to account for initially transversely isotropic material symmetry, is taken as :

$$\frac{dD_c}{dt} = C \Delta^r (1 - D_c)^{-m}$$ (10)

in which :

$$m = \frac{n\lambda}{\lambda-1} - 1$$

$$C = \frac{(\lambda-1)}{n\lambda t_0}$$

and n, r, λ and t_0 are material constants, as specified in [40,59]. For instance λ is often referred to as the creep damage tolerance and measures the ability of the metal to withstand local straining at points of high strain concentration in a structure.

12

For further information regarding the characterization of this growth law the reader is referred to [59].

If one assumes the isotropic limit, i.e., $D_{ij} = 1/3 \; \delta_{ij}$, since $D_{ii} = 1$; then,

$$I = \frac{1}{3} S_{ii} = 0$$

$$\hat{I} = \frac{1}{3} S_{ij} S_{ij}$$

(11)

and thus

$$S^2 = I_1 = \frac{1}{6} S_{ij} S_{ij} = \frac{1}{3} J_2$$

$$\mathscr{S}^2 = I_2 = \frac{1}{3} S_{ij} S_{ij} = \frac{2}{3} J_2$$

$$I_3 = 0$$

and

$$\mathscr{N} = \frac{1}{3} \sigma_{ii} + \frac{1}{\sqrt{3}} \sqrt{J}_2$$

thereby indicating that equation (8) <u>does not reduce</u> to the equation put forth by Leckie and Hayhurst, that is,

$$\Delta = \frac{1}{3\sigma_0} [\; \mathscr{A}_1 + (1+\alpha_c \; \sqrt{2}) \lceil \dot{J}_2 \;]$$

(12)

while equation (9) <u>does reduce</u> to the previous equation [8,40], if $\alpha_c = 0$, such that,

$$\Delta = \frac{1}{\sigma_0} [\beta_c \mathscr{A}_1 + (1-\beta_c) \lceil \dot{J}_2 \;]$$

(13)

as seen by comparing $\mathscr{S}$ in table I to the above.

13

4.2 Multiaxial Transversely Isotropic Fatigue Damage Model

Figure 4b is the extension of Fig. 2b and illustrates the damage, i.e., the micro and mesocracks, one might encounter on the mesostructural scale when a composite material is subjected to fatigue type loading. The approach taken to model this damage will be the stress based approach discussed earlier. Extension of these previous models (Table II) is accomplished, once again by introducing anisotropic damage surfaces with appropriate invariants [59,61,62] that represent stress states that are likely to strongly influence the various damage modes in metallic composites. For instance, we assume that i) the transverse shear stress (I_1) and thus implicitly the transverse normal stress, will dictate matrix cracking; ii) the longitudinal shear stress (I_2) dictates interfacial degradation; and iii) the maximum normal stress (I_3) in the fiber direction will dictate fiber breakage. In this way, it is believed that the following fatigue limit and static fracture surface contain the most pertinent damage producing stress measures. Similarly, a normalized stress amplitude measure can be defined. That is, let

$$F_{()} = \sqrt{\frac{1}{()_L^2} \left\{ (4\omega_{()}^2 - 1) I_1 + \frac{(4\omega_{()}^2 - 1)}{\eta_{()}^2} I_2 + 9/4 \, I_3 \right\}} \quad (14)$$

where the <u>fatigue limit surface</u>[2] is defined as ;

$$\hat{F}_{f\ell} - 1 = \frac{1}{2} \max_t \max_{t_0} F_{(f\ell)}(\sigma_{ij}(t) - \sigma_{ij}(t_0)) - 1 \quad (15)$$

the <u>static fracture surface</u> is;

$$1 - \hat{F}'_u = 1 - \max_t F_{(u)}(\sigma_{ij}(t)) \quad (16)$$

---

[2]The authors acknowledge that not all monolithic materials exhibit a maked fatigue o endurance limit, e.g., nonferrous alloys, however it is assumed (based on experimental evidence [63]) that a sufficiantly large class of composite materials will posses such a limit. Furthemore, we assert that fatigue lives beyound some specified value, say 10^7, can be considered infinite for most practical design puposes and thereby allow the assumption of an endurance limit.

and the normalized stress amplitude is;

$$\hat{F}_m = \hat{F}_m(\sigma_{ij}) = \frac{1}{2} \max_t \max_{t_0} [F_{(m)}(\sigma_{ij}(t) - \sigma_{ij}(t_0))] \qquad (17)$$

wherein the (.) in eq.(14) is to be replaced by either fl, u, or m

with

$$f\ell_L = \sigma_{f\ell_L} \;,\; \omega_{f\ell} = f\ell_L/f\ell_T \;,\; \eta_{f\ell} = \tau_{f\ell_L}/\tau_{f\ell_T} \;,\; u_L = \sigma_{u_L} \;,\; \omega_u = u_L/u_T \;,$$

$$\eta_u = \tau_{u_L}/\tau_{u_T} \;,\; m_L = M_L \;,\; \omega_m = M_L/M_T \;\text{ and }\; \eta_m = \tau_{m_L}/\tau_{m_T}$$

being material parameters, some of them varying with the mean stress, that describe the initial anisotropy of the surfaces and m_L is defined by equation (40). Note that the subscripts L and T denote, respectively, the longitudinal (in the fiber) and transverse (normal to the fiber) directions. Now with these two surfaces and normalized stress amplitude it is a straight forward task to extend the models of Table II to account for materials which posses initial transversely isotropic material symmetry. The new multiaxial representations are now given in Table IV.

One additional modification, besides the inclusion of a preferred direction, has been introduced into the fatigue models of Table IV and that is a hydrostatic stress measure (P) that combines both the Sines [64] and Crossland [65] criteria, i.e.,

$$P = \zeta \, \sigma_{Hmax} + (1 - \zeta) \, \sigma_{Havg.} \qquad (18)$$

This alternate hydrostatic measure (P) is felt to be required since a judgment as to the most applicable criteria is unavailable due to the lack of experimental data on metallic composites. In Table II, only the Sine's criteria was considered, i.e., $\zeta = 0$. Finally, if one assumes that the ratios $\omega_{f\ell}, \eta_{f\ell}, \omega_u, \eta_u, \omega_m, \eta_m$, all are equal to one then the isotropic models given in Table II are easily recovered with only a slight modification to the coefficient 'a' in models I and III and C_0 in model II.

4.2.1 Uniaxial Simplification of Model I

Due to the similarity in structure of models I, II and III and the fact that model I is the simplest to describe, only this model will be considered subsequently. Considering a uniaxial stress state (σ) and a fiber direction oriented in the X–Y plane at an angle θ from the X axis, i.e., $d_i = (\cos\theta, \sin\theta, 0)$. The following simplification of model I, cf. Table IV, is obtained;

$$J_2 = \frac{\sigma^2}{3}$$

$$I^2 = \frac{1}{9} (2 \cos^2\theta - \sin^2\theta)^2 \sigma^2 \qquad (19)$$

$$\hat{I} = \frac{1}{9} (4 \cos^2\theta + \sin^2\theta) \sigma^2$$

with

$$I_1 = \sigma^2 A_1$$

$$I_2 = \sigma^2 A_2 \qquad (20)$$

$$I_3 = \frac{4}{9} \sigma^2 A_3$$

such that

$$dD_F = [1-(1-D_F)^{\beta+1}]^\alpha \ (CC_m)^{\beta/2} \left[\frac{\sigma_{max} - \overline{\sigma}}{(1-D_F)} \right]^\beta dN \qquad (21)$$

with $\qquad \alpha = 1 - a \left\{ \dfrac{<\sqrt{CC_{f\ell}} \ (\sigma_{max} - \overline{\sigma}) - 1>}{<1 - \sqrt{CC_u} \ \sigma_{max}>} \right\} \qquad (22)$

where

$$CC_m = \frac{1}{M_L^2} \{(4\omega_m^2-1) A_1 + \frac{(4\omega_m^2-1)}{\eta_m^2} A_2 + A_3\}$$

$$CC_{f\ell} = \frac{1}{\sigma_{f\ell_L}^2} \{(4\omega_{f\ell}^2-1) A_1 + \frac{(4\omega_{f\ell}^2-1)}{\eta_{f\ell}^2} A_2 + A_3\} \qquad (23)$$

$$CC_u = \frac{1}{\sigma_{u_L}^2} \{(4\omega_u^2-1) A_1 + \frac{(4\omega_u^2-1)}{\eta_u^2} A_2 + A_3\}$$

$$A_1 = \frac{1}{3} - \frac{4}{9} \cos^2\theta - \frac{1}{9} \sin^2\theta + \frac{1}{36} (2\cos^2\theta - \sin^2\theta)^2$$

$$A_2 = \frac{4}{9} \cos^2\theta + \frac{1}{9} \sin^2\theta - \frac{1}{9} (2\cos^2\theta - \sin^2\theta)^2 \qquad (24)$$

$$A_3 = \frac{1}{4} (2\cos^2\theta - \sin^2\theta)^2$$

and henceforth,

$$<f> \begin{cases} = 0 \text{ if } f < 0 \\ = f \text{ if } f \geq 0 \end{cases}$$

with $M_L(P)$, $\sigma_{f\ell}(P)$, $\sigma_{u_L}(P)$ and the ω and η ratios are independent of σ_H since the modification factor cancels. Note once again that if $\omega_{()}$ and $\eta_{()}$ are equal to 1 (i.e., isotropy) then equations (21) and (22) become.

$$dD_F = [1-(1-D_F)^{\beta+1}]^\alpha [\frac{\sigma_{max}-\overline{\sigma}}{\overline{M}_L(1-D_F)}]^\beta dN \qquad (25)$$

and
$$\alpha = 1 - \hat{a} \frac{\left\langle \sigma_{max} - \sigma_{f\ell}(\bar{\sigma}) \right\rangle}{\left\langle \sigma_u - \sigma_{max} \right\rangle}$$
(26)

with
$$\sigma_{f\ell}(\bar{\sigma}) = \sigma_{f\ell}(0) + (1 - b\, \sigma_{f\ell}(0))\, \bar{\sigma}$$

and
$$\hat{a} = a \left[\frac{\sigma_u}{\sigma_{f\ell}} \right]$$

which are identical in form to the uniaxial ONERA model I of Table III.

Integrating equation (21) for N cycles, where σ_{max} and $\bar{\sigma}$ are held fixed leads to :

$$N = \frac{[1 - (1 - D_F)^{\beta+1}]^{(1-\alpha)}}{(1+\beta)^{(1-\alpha)}} \; [\sqrt{CC_m} \, (\sigma_{max} - \bar{\sigma})]^{-\beta}$$
(27)

If we cycle the material to failure (N_F), which is defined to occur when $D_F = 1$, we find that

$$N_F = \frac{1}{(1+\beta)\ (1-\alpha)} \; [\sqrt{CC_m} \, (\sigma_{max} - \bar{\sigma})]^{-\beta}$$
or
(28)

$$N_F = \frac{\left\langle 1 - \sqrt{CC_u} \; \sigma_{max} \right\rangle}{(1+\beta)\ a\ \left\langle \sqrt{CC_{f\ell}} \, (\sigma_{max} - \bar{\sigma}) - 1 \right\rangle} \; [\sqrt{CC_m} \, (\sigma_{max} - \bar{\sigma})]^{-\beta}$$

Now rewriting equation (27), an expression describing the accumulation of damage, for a given loading cycle, in terms of the remaining life ratio can be obtained, that is :

$$D_F = 1 - [1 - (N/N_F)^{1/(1-\alpha)}]^{1/(1+\beta)}$$
(29)

Note that the accumulation of damage is nonlinear and is also a function of fiber orientation, as is the number of cycles to failure.

18

Similarly if a two–level loading test is considered, one obtains, by integrating equation (21) in two steps, the same expression as in the case of isotropic materials i.e;

$$N_2/N_{F_2} = 1 - (N_1/N_{F_1})^p \qquad p = (1 - \alpha_2)/(1 - \alpha_1) \qquad (30)$$

Except here α_1, α_2, N_{F_1} and N_{F_2} are all dependent upon the orientation of the fibers (or conversely the load). Note that N_{F_1} and N_{F_2} are the failure lives (on the S–N curve) for the first and second loading conditions, respectively; while N_1 is the number of cycles applied at the first loading level and N_2 is the remaining life at the second level.

4.2.2 Nondimensional Uniaxial Parametric Study

In order to conveniently examine the behavior of this fatigue model in detail for a variety of composite systems the following dimensionless form has been taken. Here both the maximum and mean stress have been normalized relative to the ultimate, static fracture, stress (σ_{u_L}) in the fiber direction, i.e.,

$$S_{max} = \frac{\sigma_{max}}{\sigma_{u_L}}$$

and

$$\bar{S} = \frac{\bar{\sigma}}{\sigma_{u_L}} \qquad (31)$$

, respectively. Equations (21) and (22) can then be rewritten as:

$$\frac{dD_F}{dN} = [1-(1-D_F)^{\beta+1}]^\alpha \; (\mathscr{S}\mathscr{S}_m)^{\beta/2} \left[\frac{S_{max}-\bar{S}}{(1-D_F)}\right]^\beta \qquad (32)$$

19

with

$$\alpha = 1 - a \left\langle \frac{[\sqrt{\mathcal{GG}_{f\ell}} \ (S_{max} - \bar{S}) - 1]}{[1 - \sqrt{\mathcal{GG}_u} \ S_{max}]} \right\rangle \tag{33}$$

where

$$\mathcal{GG}_m = -\frac{1}{\mathcal{M}^2} \{(4\omega_m^2 - 1) \ A_1 + \frac{(4\omega_m^2 - 1)}{\eta_m^2} A_2 + A_3\}$$

$$\mathcal{GG}_{f\ell} = -\frac{1}{\mathcal{R}^2} \{(4\omega_{f\ell}^2 - 1) \ A_1 + \frac{(4\omega_{f\ell}^2 - 1)}{\eta_{f\ell}^2} A_2 + A_3\} \tag{34}$$

$$\mathcal{GG}_u = \{(4\omega_u^2 - 1) \ A_1 + \frac{(4\omega_u^2 - 1)}{\eta_u^2} A_2 + A_3\}$$

$$\mathcal{M} = \frac{M_L}{\sigma_{u_L}}$$

$$\tag{35}$$

$$\mathcal{R} = \frac{\sigma_{f\ell_L}}{\sigma_{u_L}}$$

and A_1, A_2 and A_3 are those defined previously. Again integrating equation (32) one obtains expressions relating, i) the number of cycles to failure relative to the applied normalized stress,

$$N_F = \frac{[\sqrt{\mathcal{GG}_m} \ (S_{max} - \bar{S})]^{-\beta}}{(1+\beta) \ a} \left\langle \frac{[1 - \sqrt{\mathcal{GG}_u} \ S_{max}]}{[\sqrt{\mathcal{GG}_{f\ell}} \ (S_{max} - \bar{S}) - 1]} \right\rangle \tag{36}$$

and ii) the damage accumulation relative to the ratio of remaining life:

$$D_F = 1 - [1 - (N/N_F)^{1/(1-\alpha)}]^{1/(1+\beta)} \tag{37}$$

4.2.2.1 Direction Independent Parameters

First, considering an isotropic material, i.e., $w_{()} = \eta_{()} = 1$, the effect of varying the parameters $\mathcal{R}$, $\mathcal{M}$, β, a, and the mean stress ($\overline{S}$) on the S–N curve will be examined. To simplify and yet not limit the study, the parameters $\sigma_{f\ell}$ and M_L will be taken to be independent of hydrostatic stress, that is to say b and b' (given in Table IV) are zero. The baseline values assumed are those corresponding to 304 stainless steel (see Table V and Fig. 5) and have been obtained from Lemaitre and Chaboche [12]. Due to the assumption of material isotropy, equation (36) can be simplified to:

$$N_F = \frac{1}{(1+\beta)\,a}\left[\frac{S_{max}-\overline{S}}{\mathcal{M}}\right]^{-\beta}\left\langle\frac{[1-S_{max}]\,\mathcal{R}}{[S_{max}-(\overline{S}+\mathcal{R})]}\right\rangle \qquad (38)$$

Now as suggested by equation (38), if either the mean stress ($\overline{S}$) or fatigue ratio ($\mathcal{R}$) are modified, the load level at which an endurance limit is reached is also changed. This is clearly shown in Figs. 6 and 7, where mean stress values of,

$\overline{S} = 0.0, 0.2, 0.4$ and 0.6 and fatigue ratio values of $\mathcal{R} = 0.1, 0.25, 0.4, 0.55$ and 0.7 are considered, respectively, while all other parameters are held fixed at the baseline values given in Table V. In both cases, as the value is increased so is the endurance level.

Translation of the S–N curve is achieved, as indicated by equation (38), by varying the parameter $\mathcal{M}$ (i.e., $\mathcal{M} = 1.125, 2.25, 4.5$ and 9.0) and 'a' (i.e., a = 0.01, 0.1, 0.5, 1.0, and 2.0) as shown in Figs. 8 and 9, respectively; while again holding all other parameters fixed. It is clear that increasing $\mathcal{M}$ shifts the S–N curve to the right (increases the number of cycles to failure at a given load) while increasing 'a' shifts the S–N curve to the left (decreases the number of cycles to failure at a given load). Thus only the product (a $\mathcal{M}^{-\beta}$), and not the individual values of a and $\mathcal{M}$, is important in determining the life at a given load level. However, the actual value of 'a' does strongly affect the damage accumulation and therefore if any other type of damage (e.g. creep) is present, both parameters $\mathcal{M}$ and 'a' need to be determined explicitly.

Finally, equation (38) indicates that modifying the parameter β will both translate the S–N curve and affect the abruptness of the transition from infinite life to immediate failure. Clearly, β equal to zero is the lower limit and will give the most abrupt S–N curve for a fixed set of material parameters. Figure 10 illustrates the effect of varying β, were $\beta = 0.5$, 1.0, 3.0, 5.0 and 7.0 are considered.

4.2.2.2 Parameters Defining the Initial Transverse Isotropy.

Considering the assumed baseline transversely isotropic material parameters given in Table V, the modification of the S–N curve with fiber orientation (or equivalently, load orientation relative to a fixed fiber orientation) is examined in Fig. 11. As one might suspect, (as a composite material is designed to be stronger when loaded parallel to the fiber direction) both the static fracture strength and fatigue limit are reduced with an increase in fiber orientation. The amount of decrease in load carrying ability is clearly dependent upon the "degree" of anisotropy and is represented in this fatigue damage model by the ω and η ratios in the ultimate stress ($\mathscr{S}\mathscr{C}_u$), fatigue limit ($\mathscr{S}\mathscr{C}_{f\ell}$) and normalizing stress amplitude ($\mathscr{S}\mathscr{C}_m$), see equations (36). Note that in the baseline material parameter set, all three anisotropic functions are considered to have the same degree of initial anisotropy. In this section an examination of the impact of perturbing the various anisotropic measures will be undertaken.

Equations (34–36) and (24) indicate that the angle dependency is manifested through the functions A_1, A_2, and A_3 which are associated with the longitudinal shear, transverse shear and normal stress components, respectively. This angle dependency is clearly shown in Fig. 12. At $\theta=0°$ both the longitudinal and transverse shear components are zero; at $\theta=45°$ the longitudinal shear stress component is a maximum and the transverse shear and longitudinal normal stress are equal; at $\theta=57°$ the longitudinal normal stress is zero and at $\theta=90°$ the transverse shear and longitudinal normal stress are equal. Figure 12 clearly indicates that when $\theta=0°$, changes in any of the measures of anisotropy (i.e., ω's or η's) will have no affect since both the A_1 and A_2 expressions are equal to zero. Similarly, when $\theta=90°$, any change in the shear "strength" measures (i.e., η's) will not have any impact in the resulting S–N curves. Thus suggesting, that initial characterization of material parameters a, b, β, $\mathscr{R}$ and $\mathscr{M}$ should be conducted with longitudinally reinforced and loaded specimens.

4.2.2.3 Variation of ω_u, $\omega_{f\ell}$ and ω_m.

Figure 13 illustrates the effect of varying the ultimate strength ratio $(\omega_u = \sigma_{u_L}/\sigma_{u_T})$ on the S–N curve corresponding to a fiber orientation of $\theta=15°$. The values of ω_u are taken to be 2, 4, 5, 8 and 16, while all other parameters are held fixed at the baseline values given in Table V. As one might expect increasing the ultimate strength ratio affects only the low cycle fatigue portion of the curve (by decreasing the static fracture stress) while the endurance limit remains unaffected. Conversely, increasing the fatigue limit ratio (i.e., $\omega_{f\ell} = $ 2, 4, 5, 8 and 16), while holding all other parameters fixed, decreases the endurance limit while leaving the ultimate strength unchanged. See Fig. 14 for an example at a fiber orientation of 15 degrees. The impact of changing ω_u from 5.0 to 3.0 for fiber orientations of 0, 15, 30, 60 and 90 is shown in Fig. 15. Comparing Figs. 11 and 15 one observes a similar trend (as that observed in Fig. 13) for all angles except $\theta=0°$, which remains unaffected for reasons indicated earlier. Note that although the present model provides significant flexibility, in that ω_u and $\omega_{f\ell}$ can be varied independently; in reality one would expect a relationship to exist between the ultimate strength and the endurance limit, thus placing restrictions on the ranges of these parameters.

Furthermore, by varying the normalizing stress ratio ω_m, a horizontal translation of the transition portion of the S–N curve can be obtain while the ultimate stress and fatigue limit remain unchanged. An example is shown in Fig. 16 where ω_m takes on the values of 2, 4, 5, 8 and 16, assuming a fiber orientation of 15 degrees, while all other parameters once again remain fixed. Clearly, increasing the ratio shifts the S–N curve to the left (decreasing the number of cycles to failure for a given load).

Thus, by merely assuming different degrees of anisotropy for the three functions $\mathscr{GG}_u$, $\mathscr{GG}_{f\ell}$ and $\mathscr{GG}_m$, i) either end of the S–N curve can be modified while leaving the other end unchanged, or ii) the center portion can be horizontally translated, while the ultimate and fatigue limit stresses remain unchanged. This suggests that the model has sufficient flexibility to fit a broad class of materials.

The impact of varying the degree of anisotropy, for example ω_u, on the S–N curve can be seen for all angles of fiber orientation by plotting the functions $\sqrt{\mathscr{GG}_{f\ell}}$ and $\sqrt{\mathscr{GG}_u}$, $\sqrt{\mathscr{GG}_m}$. In Fig. 17 only $\sqrt{\mathscr{GG}_u}$ has been shown versus angle of orientation θ, as the other two functions will have similar behavior, except for being

scaled by a multiplying factor. Examining Fig. 17 it is evident that for a specified ratio ω_u the function $\sqrt{\mathscr{G}\mathscr{G}_u}$ increases as one increases the angle θ; however, depending upon the magnitude of ω_u an angle can be found where this increase is at a decreasing rate. This explains why, for larger angles, one sees an incrementally smaller change in the response curve with increasing angle (i.e., variation in the S–N curve), see Figs. 11 and 15. Finally, one more important point can be discerned from Fig. 17, and that is the need for the ratio ω to always be greater than or equal to η since if $\omega < \eta$ a minimum occurs in the function at an angle other than zero, which violates physical reasoning.

4.2.2.4 Variation of η_u, $\eta_{f\ell}$ and η_m.

Variation of the shear ratios η_u, $\eta_{f\ell}$, and η_m has a similar impact on the overall trends, but not actual magnitudes, of the S–N curve, as did their respective normal stress ratios. Examples involving the variations of each ratio (for values of 1, 2, 4, and 5) with a fiber orientation of 15 degrees are shown in Figs. 18, 19 and 20, respectively. The interaction between the shear strength and the normal strength ratio are shown in Fig. 21, for an $\omega_u=5.0$, and in Fig. 22, for an $\omega_u=16.0$, when the η_u ratio takes on values of 1, 1.5, 2, 3, 4, and 5 in the case of Fig. 21 and 1.0, 1.5, 2, 4, 8, and 16 in the case of Fig. 22. Note how in both cases (i.e., $\omega_u=5.0$ and $\omega_u=16.0$) the shape of the function $\mathscr{G}\mathscr{G}_u$ is greatly affected, particularly for low values of η. Also it is clear that when $\eta=1$ a maximum at some intermediate angle is obtained. The ramification of this intermediate maximum is unknown at this time. As with the cases involving the normal stress ratios, ω_u and $\omega_{f\ell}$, one would expect that a relationship would exist between η_u and $\eta_{f\ell}$ such that the practical ranges of these parameters are not independent.

4.2.3 Required Exploration and Characterization Experiments.

Here, the determination of the various material parameters will be discussed.

Fatigue of Isotropic Material

Considering first the case of isotropic materials, it is assumed that S–N curves (shown schematically in Fig. 23) exist for different stress ratios ($R=\sigma_{min}/\sigma_{max}$) and that the ultimate static fracture strength (σ_u) is known. Given this data, one may

24

then obtain a plot of fatigue limit (σ_ℓ) versus mean stress $(\overline{\sigma})$, as shown in Fig. 24, from which the material parameter b can be easily found. Note that a linear dependence is assumed in Fig. 24; this, however, may not be sufficient to describe the material and one might have to consider an alternative representation.

Rewriting the isotropic simplification of equations (23) and (28) and taking the natural logarithm of both sides, one can obtain the following expression :

$$\ln\left[\left\langle\frac{\sigma_m - \sigma_1}{\sigma_u - \sigma_m}\right\rangle N_F\right] = \ln\left[\frac{1}{a(1+\beta) M^{-\beta}}\right] - \beta \ln(\sigma_m - \overline{\sigma}) \tag{39}$$

or
$$Y = Y_0 - \beta X$$

Now plotting Y versus X (see Fig. 25) and fitting a straight line through the data, the material parameter β is obtained from the determined slope and the product (a $M^{-\beta}$) may be determined from the intercept. Similarly solving equations (23) and (28) for M, i.e.,

$$M = (\sigma_m - \overline{\sigma}) [N_F (1+\beta) (1-\alpha)]^{1/\beta}$$

or
$$M = (\sigma_m - \overline{\sigma}) [N_F (1+\beta) a \left\langle\frac{(\sigma_m - \overline{\sigma}) - \sigma_{f1}}{\sigma_u - \sigma_m}\right\rangle \frac{\sigma_u}{\sigma_{f1}}]^{1/\beta} \tag{40}$$

It becomes apparent that M represents a normalizing factor such that it ensures a certain life (N_F^a) for a specified stress amplitude, $\sigma_a = (\sigma_m - \overline{\sigma})$, see Fig. 26. Clearly, M is also dependent upon the slope β and the material constant a, thus leading one to the conclusion that the remaining life measurements are insufficient to completely characterize the damage evolution equation, i.e., the value of 'a'. Only the product (a $M^{-\beta}$) may be determined directly, by either, using the previous Y intercept (Y_0) of Fig. 25, i.e.;

$$a M^{-\beta} = \frac{1}{(1+\beta) e^{Y_0}} \tag{41}$$

or selecting a point on the S–N curve (see Fig. 23 or 26) such that

$$a \, M^{-\beta} = \frac{\sigma_a^{-\beta} \, <\sigma_u - \sigma_m> \, \sigma_{f\ell}}{N_F \, (1+\beta) \, <\sigma_a - \sigma_{f\ell}> \, \sigma_u} \quad . \tag{42}$$

This indeterminacy (lack of independence between 'a' and M) has been shown not to be important, as long as only fatigue damage accumulation is considered, even under complex loading histories. However, in the case, for example, of creep–fatigue interaction the complete characterization (independent measurement of parameter 'a') of the model is required.

To accomplish this, an indirect measurement of damage accumulation can be obtained from the change in the stress–strain response during the fatigue process using the effective stress concept. One method of experimentally measuring the damage accumulation is to monitor the change in elastic response (Young's Modulus) with applied cycles of stress, that is

$$D = 1 - \frac{\hat{E}}{E} \tag{43}$$

where $\hat{E}$ is the effective (current) modulus and E is the initial one. A number of researchers have used this procedure for both metallic and composite materials [15,31,34] and in fact such measurements have been observed to correlate well with quantitative micro–crack evaluations as well [42,43]. Now given D as a function of remaining cycles (N/N_F), all that is required to determine 'a' is to plot the natural logarithm of D versus that of N/N_F, as shown in Fig. 27, calculate the average slope Z for various stress amplitudes, and solve for 'a', i.e.;

$$a = \frac{(1+\beta) \, <\sigma_u - \sigma_m>}{Z \, <\sigma_a - \sigma_{f\ell}> \, \sigma_u} \, \sigma_{f\ell} \tag{44}$$

With this, all material parameters, i.e., a, β, b, σ_u, $\sigma_{f\ell}$ and M, have been determined in the case of isotropic materials.

If model II is selected, the function describing the influence of frequency needs to be characterized, that is:

26

$$N_i = \cfrac{C_0}{1 + \left[\cfrac{\nu_0}{\nu}\right]^\gamma} \left[\frac{<\sigma_m - \sigma_{\ell i}(\overline{\sigma})>}{<\sigma_u - \sigma_m>} \right]^{-\beta_i}$$

This is accomplished by plotting semi–logarithmically N_i versus $(\sigma_m - \sigma_{\ell i})/(\sigma_u - \sigma_m)$ for a variety of frequencies; where N_i is obtained by making use of the empirical expression put forth by Manson [66], that is,

$$N_i = N_F - 14 \, N_F^{0.6}$$

Thus the intercept gives $C(\nu)$ while the slope is $-\beta_i$. Now plotting $C(\nu)$ versus ν and rewriting the expression for $C(\nu)$, for example

$$C(\nu) = \cfrac{C_0}{1 + \left[\cfrac{\nu_0}{\nu}\right]^\gamma} = C_0 - \nu_0^\gamma \, \frac{C(\nu)}{\nu^\gamma}$$

and plotting $C(\nu)$ versus $C(\nu)/\nu^\gamma$ we see that ν_0^γ and C_0 are the slope and intercept, respectively, given a value for γ. The point here is to plot a number of curves corresponding to different γ's and selecting the one that best fits the data. This procedure is described in greater detail in reference [25].

Fatigue for Transversely Isotropic Materials

For transversely isotropic materials, e.g., hexagonally packed unidirectional composite materials, the determination of the material properties follow a similar process, except now additional testing is required both in tension and torsion in the longitudinal and transverse directions, to define the extent of initial anisotropy, i.e., the ratios ω_u, η_u, $\omega_{f\ell}$, $\eta_{f\ell}$ and ω_m, η_m. Figure 28 illustrates schematically the expected S–N curves for a composite material loaded longitudinally ($\theta=0°$) and trans–versely ($\theta=90°$) at a given mean–stress. Given such data, as well as the associated shear S–N curves, the various ω and η ratios can be determined. Note that in the present theory β, a and b are assumed to be independent of fiber orientation (i.e., d_i). This assumption may need to be modified if experimental evidence suggests otherwise, therefore during the initial exploration and characterization of a class of composite systems the procedures illustrated by Figs. 24, 25, and 27 should be

27

repeated four times, that is for the case of normal and shear type loadings in the longitudinal as well as transverse directions.

Clearly the above discussion suggests a significant, and potentially quite expensive, experimental program. This experimental program may however be able to be reduced and augmented through numerical simulation using a suitable homogenization technique with periodic boundary conditions. Furthermore utilization of the homogenization technique should allow micro–mechanical effects (e.g., bond strength, volume fraction, etc...) to be included in this phenomenological theory, through the parameters, σ_{u_L}, $\sigma_{f\ell_L}$, ω_u, η_u, $\omega_{f\ell}$ and $\eta_{f\ell}$.

One important micromechanical aspect which has been intentionally neglected in this initial formulation is the role of residual stresses (which are expected to be significant) in the life of metallic composites. However, at this time insufficient experimental data exist to verify the various extensions of the presently described models, let alone admit the introduction of further complicating factors. Therefore this aspect will be addressed in future work.

Creep During Cyclic Loading for Isotropic Materials

A final remark regarding the characterization of the required material parameters. The parameter τ in the rate form of the delay stress equation in Table I, can be obtained most easily by assuming a sinusoidal loading history. For example in uniaxial form the required equation set is

$$\sigma = A \sin \omega t$$
$$X = C \sin (\omega t + \varphi)$$
$$\frac{dX}{dt} = (\sigma - X)/ \tau$$
$$\omega = 2\pi \nu$$

and the solution is

$$X = \frac{A}{(1 + \tau^2 \omega^2)}[\sin \omega t - \tau \omega \cos \omega t]$$

An expression relating the maximum delayed stress (X_{max}) to the maximum applied stress (σ_{max}),

28

$$X_{max} = \frac{\sigma_{max}}{(1 + \omega^2 \tau^2)^{0.5}}$$

and is obtained by finding the stationary point of the above equation. Now assuming that $X_{max} = \sigma_{mean}$ at a sufficiently high frequency of loading , an expression defining τ is obtained

$$\tau = \frac{1}{2\pi \nu} \{ (\sigma_{max}/\sigma_{mean})^{0.5} - 1.0 \}$$

Clearly, the suitability of this frequency dependence should be examined when the load history is a fully–reversed one.

4.3 CREEP–FATIGUE INTERACTION

Figure 4c is the extension of Fig. 2c and illustrates schematically the interaction of intergranular and transgranular defects. As for isotropic models it is surmised that the presence of cavities allow for easier crack propagation and that the increase in stress intensity at a crack tip causes an increase in the nucleation and coalescence of voids.

Analytically this interaction is again represented using the effective stress concept, by assuming that the mechanical effects of creep and fatigue damage can be directly added, (see equation (5)). Thus the two functions (f_c and f_F) can be determined independently from pure tensile creep tests and pure high frequency fatigue tests.

It is primarily in this context (creep/fatigue interaction) that the main distinctions between models I, II and III of Table IV can be observed.

5.0 CONCLUSIONS

Three isothermal multiaxial continuum damage mechanics models for the creep, fatigue, and creep/fatigue interaction of a unidirectional metal matrix composite volume element have been presented. The intended applications are reinforced structures in which the fiber direction may vary throughout but a single fiber direction can be identified locally (local transverse isotropy) within a given volume element. Each model is phenomenological, with varying degrees of complexity to

accurately predict the initiation and propagation of intergranular and transgranular defects over a wide range of loading conditions.

The development of these models are founded on the definition of an initially transversely isotropic fatigue limit surface, static fracture surface, normalized stress amplitude function and isochronous creep damage failure surface, from which both fatigue and creep damage evolutionary laws can be obtained. The anisotropy of each model is defined through physically meaningful invariants reflecting the local stress and material orientation. All three transversely isotropic models have been shown, when taken to their isotropic limit, to directly simplify to previously developed and validated creep and fatigue continuum damage theories.

Results of a nondimensional parametric study illustrates i) the flexibility of the present formulation when attempting to characterize a large class of composite materials and ii) its ability to predict anticipated qualitative trends in the fatigue behavior of unidirectional metal matrix composites. Additionally, the potential for the inclusion of various micromechanical effects (e.g. bond strength, volume fraction, etc.), into the phenomenological anisotropic parameters have been noted, as well as a detailed discussion regarding the necessary exploratory and characterization experiments needed to utilize the featured damage theories.

Two potential drawbacks to the present formulation are i) the scalar damage measure employed and ii) the expensive experimental program required. Future work in this area will include the examination of the utility of the present formulation to predict high temperature applications, the initiation of an experimental characterization and validation program and the numerical implementation into a post processing life prediction computer code.

APPENDIX A – NOMENCLATURE

Stresses:

σ_{ij} is the Cauchy stress tensor

σ^d_{ij} is the delayed stress tensor

σ^d is the uniaxial delayed stress

S_{ij} is the deviatoric stress tensor

S_{max} is the normalized uniaxial maximum stress

$\bar{S}$ is the normalized uniaxial mean stress

$\bar{\sigma}$ is the uniaxial mean stress

σ_m is the uniaxial maximum applied stress

σ_a is the applied stress amplitude, i.e., $\sigma_m - \bar{\sigma}$

σ_{Havg} is the uniaxial mean hydrostatic stress

σ_{Hmax} is the uniaxial maximum hydrostatic stress

$\tilde{\sigma}$ is the uniaxial effective stress

σ_0 is the reference stress

Invariants:

J_0 is the stress invariant representing the maximum principal stress

$\mathscr{J}_1$ is the first invariant of the total stress (hydrostatic stress)

J_2 is the second invariant of the deviatoric stress (expressed for shear)

$\tilde{J}_2$ is the second invariant of the deviatoric stress (expressed for normal stress)

I_1 is the invariant representing transverse shear stress

I_2 is the invariant representing longitudinal shear stress

I_3 is the invariant representing the maximum normal stress in the fiber direction

$\mathscr{N}$ is the invariant representing maximum transverse tensile stress

S is the square root of I_1

$\mathscr{S}$ is the square root of I_2

$\mathscr{A}_2$ is the invariant representing the total stress in the fiber direction

$\mathscr{A}_1$ represents the maximum amplitude in stress

$\mathscr{A}_2$ represents the avaraged mean stress

$\mathscr{A}_3$ represents the maximum octahedral stress

Material Parameters:

Creep Damage

α_c, β_c are the coefficients indicating the strength of contribution for the J_o and $\mathscr{J}_1$ invariants, respectively.

A_c is the creep damage normalizing factor

r,k are the exponents in the creep damage evolution equation

τ is related to the response time of the material

Fatigue Damage

$\mathscr{M}$ is the ratio of stress amplitude constant to static fracture stress

$\mathscr{R}$ is the ratio of endurance limit to static fracture stress

$\sigma_{f\ell}, \sigma_\ell$ is the normal stress endurance limit

σ_u is the ultimate normal stress or static fracture stress

M is the normalizing stress amplitude

τ_u is the ultimate shear stress or static fracture stress

$\tau_{f\ell}$ is the shear stress endurance limit

$\sigma_{\ell i}$ is the uniaxial initiation endurance limit

$\sigma_{\ell p}$ is the uniaxial propagation endurance limit

$S_{o\ell}, \sigma_{o\ell}$ are the initial multiaxial and uniaxial endurance limits, respectively

S_{oi}, σ_{oi} are the initial multiaxial and uniaxial initaition limit stresses, respectively

S_{op}, σ_{op} are the initial multiaxial and uniaxial propagation limits, respectively

ω_m is the ratio of longitudinal to transverse normalizing normal stress amplitude

ω_u is the ratio of longitudinal to transverse ultimate normal stress

$\omega_{f\ell}$ is the ratio of longitudinal to transverse normal fatigue or endurance limit stress

η_u is the ratio of longitudinal to transverse shear static fracture stress

$\eta_{f\ell}$ is the ratio of longitudinal to transverse shear fatigue limit stress

η_m is the ratio of longitudinal to transverse shear normalizing stress amplitude

$a, \hat{a}$ is the scaling factor for the stress dependency in the fatigue damage exponent

b, b', b'' are parameters indicating the effect of mean stress

α is the fatigue damage variable exponent which can be a function of stress

β is the exponent on the normalized stress amplitude

β_i is the exponent on the normalized stress amplitude during initiation

θ is the angle between the fibers and coordinate axis

ν is the frequency of the applied loading cycles

ν_o is the reference load frequency

γ is the exponent of the frequency term

C_0 is a pre–multiplying parameter in the initiation section of model II

E Undamaged Young's Modulus

$\bar{E}$ Damaged Young's Modulus

$(\ )_L$ subscript denotes longitudinal properties

$(\ )_T$ subscript denotes traverse properties

Miscellaneous:

d_i is the unit vector denoting the local fiber direction

$D_{ij} = d_i d_j$ is the second order direction tensor

δ_{ij} is the Konecker delta function

Δ is the isochronous creep damage failure surface

D is the scalar variable representing damage

D^* is an alternate damage variable that can be used interchangably with D

D_c is the creep damage measure

D_F is the fatigue damage measure

$\hat{F}_{f\ell}$ is the fatigue limit surface

$\hat{F}_u$ is the static fracture surface

$\hat{F}_m$ is the normalized stress amplitude

P is the combined hydrostatic mean stress measure

ζ is the parameter in P, weighting the influence of the maximum hydrostatic stress

N is the variable denoting number of cycles

N_F is the number of cycles to failure

N_i is the number of cycles to crack initiation

N_p is the number of cycles for crack propagation

ω is the frequency of loading

t is time

T is temperature

$<\ >$ are the Maclaurin brackets

$H(\ )$ is the Heavyside step function

$\mathscr{F}$ is the isochronous creep damage failure surface perposed by Leckie and Hayhurst

A is the area on a face of a representative volume element

$\bar{A}$ is the effective area on a face of a representative volume element

A_D is the damaged area on the face of a representative volume element

φ is the phase shift in the sinusoidal load history

REFERENCES

1) Eshelby, J. D., "The Determination of the Elastic Field of an Ellipsoidal Inclusion and Related Problems," Proc. R. Soc. A241, 1957, pg. 376.

2) Mura, T., <u>Micromechanics of Defects in Solids</u>, M. Nijhoff, The Hague, The Netherlands, 1982.

3) Budiansky, B., "Micromechanics II," in : Proc. 10th U.S. National Congress of Applied Mechanics, J.P. Lamb (ed.), ASME, New York, 1987, pg. 25.

4) Krajcinovic, D. and Sumarac, D., "Micromechanically Based Damage Models," in : Proc. 10th U.S. National Congress of Applied Mechanics, J.P. Lamb (ed.), ASME, New York, 1987, pg. 115.

5) Nemat-Nasser, S., "Micromechnically Based Constitutive Modeling of Inelastic Response of Solids," in : Constitutive Models of Deformation, J. Chandra and R.P. Srlvastava (eds.), SIAM Publ., 1987, pg. 120.

6) Sanchez-Palenzia, E. and Zaoui, A., <u>Homogenization Techniques for Composite Media</u>, Springer, Berlin, 1987.

7) Kachanov, L.M., <u>Introduction to Continuum Damage Mechanics</u>, Martinus Nijhoff, Dordrecht, The Netherlands, 1986.

8) Leckie, F.A. and Hayhurst, D.R.,"Creep Rupture in Structures," Proc. R. Soc. Lond., 1974, pp.

9) Janson, J., "A Continuum Damage Approach to the Fatigue Process," Eng. Fract. Mech., 10, pg.651.

10) Chaboche, J.L. and Lesne, P.M., "A Non-Linear Continuous Fatigue Damage Model," Fatigue Fract. Engng. Mater. Struct., Vol. 11, No. 1., 1988, pp.1-7.

11) Chaboche, J.L., "Phenomenological Aspects of Continuum Damage Mechanics," Materials and Engineering Design : The Next Decade, B.F. Dyson, D.P. Hayhurst (Eds.), Institute of Metals, 1989, pp. 352-365.

12) Lemaitre, J. and Chaboche, J.L., <u>Mechanics of Solid Materials</u>, Cambridge University Press, 1990.

13) Hayhurst D.R., "Creep Rupture Under Multiaxial State of Stress," J. Mech. Phys. Solids, Vol. 20, No. 6, 1972, pp. 381-390.

14) Krajcinovic, D. and Fonseka, G.U., "The Continuous Damage Mechanics of Brittle Materials - Parts I and II," J. Appl. Mech., Vol. 48, 1981.

15) Talreja, R., "A Continuum Mechanics Characterization of Damage in Composite Material," Proc. R. Soc. Lond., A399, 1985, pp. 195-216.

16) Leckie, F.A. and Onat, E.T., "Tensorial Nature of Damage Measuring Internal Variables," IUTAM Symp. on Physical Non–Linearities in Structural Analysis, Springer, 1980.

17) Murakami, S. and Ohno, N., "A Continuum Theory of Creep and Creep Damage," Creep of Structures, A.R.S. Ponter (ed.), IUTAM Symp., Springer, pg. 422.

18) Chaboche J.L., "Continuum Damage Mechanics : Part I – General Concepts," J. Appl. Mech., Vol. 55, 1988, pp. 59–64.

19) Chaboche J.L., "Continuum Damage Mechanics : Part II – Damage Growth, Crack Initiation and Crack Growth," J. Appl. Mech., Vol. 55, 1988, pp. 65–72.

20) Krajcinovic, D., "Continuum Damage Mechanics," Appl. Mech. Reviews, Vol. 37, No. 1, 1984, pp. 1–6.

21) Krajcinovic, D., "Damage Mechanics," Mech. of Materials, Vol. 8, 1989, pp. 117–197.

22) Hult, J.,"Continuum Damage Mechanics (CDM) – A New Design Tool," Materials and Engineering Design : The Next Decade, B.F. Dyson, D.R. Hayhurst (eds), Institute of Metals, 1989, pp. 199–204.

23) Rabotnov, Y.N., Creep Problems in Structural Members, North Holland, Amsterdam, 1969.

24) Rabier, P.J., "Some Remarks on Damage Theory," Int. J. Engng. Sci.,Vol. 27, No. 1, 1989, pp. 29–54.

25) Lesne, P.M. and Savalle, S. ,"A Differential Damage Rule with Microinitiation and Micropropagation," Rech. Aerosp., No. 2, 1987, pp. 33–47.

26) Lesne, P.M. and Cailletaud, G., "Creep–Fatigue Interaction under High Frequency Loading," 5th Int. Conf. in Mechanical Behavior of Materials, Beijing, China, 1987.

27) Chaboche, J.L., "Fracture Mechanics and Damage Mechanics : Complementary of Approches," Int. Conf. on Numerical Methods in Fracture Mechanics, San Antonio, Pineridge Press, 1987, pp. 308–324.

28) Chaboche, J.L., "Continuous Damage Mechanics. A Tool to Describe Phenomena Before Crack Initiation," Nuclear Engineering and Design, Vol. 64, 1981, pp. 233–247.

29) Krempl, E., "On Phenomenological Failure Laws for Metals Under Repeated and Sustained Loading (Fatigue and Creep)," Conf. on Environmental Degradation of Engineering Materials, Blacksburg, VA., 1977.

30) Duvaut, G., "Analyses Fonctionnelle – Mecanique des Milieux Continus – Homogeneisation," Theoretical and Applied Mechanics, North Holland, Amsterdam, 1976.

31) Lemaitre, J., "A Continuum Damage Mechanics Model for Ductile Fracture," ASME, J. Engng. Mat. and Technology, Vol. 197, 1985, pp. 83–89.

32) Lemaitre, J. and Chaboche, J.L., "Aspect Phenomenologique de la Rupture par Endommagement," J. Mecanique Appliquee, Vol. 2, No. 3, 1978, pp. 317–365.

33) Plumtree, A. and Nilsson, J.O., "Damage Mechanics Applied to High Temperature Fatigue," Int. Spring Meeting "Fatigue at High Temperature," Paris, 1986.

34) Charewicz, A. and Daniel, I.M., "Fatigue Damage Mechanics and Residual Properties of Graphite/Epoxy Laminates," IUTAM Symp. on Mechanics of Damage and Fatigue, Haifa, Israel, 1985.

35) Greenwood, G., "Creep Life and Ductility," Int. Congress on Metals, Cambridge, Microstructure and the Design of Alloys 2, 1973, pg. 91.

36) Dyson ,B.F., "Constrained Cavity Growth, Its Use in Quantifying Recent Creep Fracture Experiments," Canadian Met. Quart., Vol. 18, 1979, pg. 31.

37) Hayhurst, D.R., "On the Role of Creep Continuum Damage in Structural Mechanics," Engineering Approaches to High Temperature Design, Wilshire and Owen (Eds.), Pineridge Press, Swansea, 1983.

38) Kachanov, L.M., "Time of the Rupture Process Under Creep Conditions," Izv. Akad. Nauk. SSR, Otd. Tekh. Nauk., Vol. 8, 1958, pp. 26–31.

39) Chaboche, J.L., "Anisotropic Creep Damage in the Framework of Continuum Damage Mechanics," Nuclear Engng. and Design, Vol. 19, 1984, pp. 309–319.

40) Leckie, F.A., "The Constitutive Equations of Continuum Creep Damage Mechanics," Phil. Trans. R. Soc. Lond. A., Vol. 288, 1978, pp. 27–47.

41) Leckie, F.A., "The Micro– and Macromechanics of Creep Rupture," Eng. Fract. Mech., Vol. 25, No. 5/6, 1986, pp. 505–521.

42) Cailletaud, G. and Levaillant, C., "Creep–Fatigue Life Prediction : What about Initiation ?," Nucl. Engng. Design., Vol. 83, 1984, pp. 279–292.

43) Hua, C.T. and Socie, D.F., "Fatigue Damage in 1045 Steel Under Constant Amplitude Biaxial Loading," Fatigue Engng. Mater. Struct., Vol. 7, No. 3, 1984, pp. 165–179.

44) Socie, D.F., Fash, J.W. and Leckie, F.A., "A Continuum Damage Model For Fatigue Analysis of Cast Iron," ASME, Conf. in Life Prediction, Albany, N.Y., 1983.

45) Chaudonneret, M. and Chaboche, J.L., "Fatigue Life Prediction of Notched Specimens," Int. Conf. on Fatigue of Engng. Materials and Struct., Sheffield, 1986.

46) Manson, S.S., "Some Useful Concepts for the Designer in Treating Cumulative Damage at Elevated Temperature," I.C.M. 3, Cambridge, Vol. 1, 1979, pp. 23–45.

47) Subramanyan, S., "A Cumulative Damage Rule Based on the Knee Point of the S–N Curve," Trans. ASME, J. of Mater. Technology, Vol.???, 1976, pp. 316–321.

48) Hashin, Z. and Laird, C., "Cumulative Damage Under Two Levels Cycling : Some Theoretical Predictions and Test Data," Fatigue of Engineering Materials and Structures, Vol. 2, 1980, pp. 345–350.

49) Chaboche, J.L., "Une Loi Differentielle d'Endommagement de Fatigue avec Cumulation non Lineaire," Revue Francaise de Mecanique, No. 50–51, 1974, English Translation in Annales de l'ITBTP, 1977.

50) Lemaitre, J. and Plumtree, A., "Application of Damage Concepts to Predict Creep–Fatigue Failures," ASME, J. of Engng. Mater. and Technology, 1979, pp. 284–292.

51) Del Puglia, A. and Vitale, E., "Damage Concept in Creep–Fatigue : Current Theories and Applications," Inelastic Analysis and Life Prediction at Elevated Temperature, ASME–PUP 59, No. 216, 1982.

52) Cailletaud, G. and Chaboche, J.L., "Lifetime Prediction in 304 S.S. by Damage Approach, ASME, paper No. 82, PVP–79, 1982.

53) Bathias, C. and Bailon, J.P., La Fatigue des Materiaux et des Structures, Paris, Maloine ed., 1981.

54) Klesnil, M. and Lukas, P., Fatigue of Metallic Materials, Amsterdam and New York, Elsevier ed., 1980.

55) Gabb, T.P., Gayda, J. and Mackay, R.A.,"Nonisothermal Fatigue Degradation of Sic/Ti Composite," Hitemp Rewiev 1990, CP 10051, 1990, pp. 32:1–12.

56) Verrilli, M., Fatigue and Fracture Branch, NASA Lewis Research Center, Cleveland, Ohio, Private communication, 1991.

57) Gayda, J., Gabb, T.P., and Lerch, B.A., "The effects of Environment on The Fatigue Life of SiC/Ti–15–3 Composites," presented at the 6th TMF Workshop, NASA Lewis Research Center, June 1991.

58) Talreja, R., Fatigue of Composite Materials, Technomic Pub., 1987

59) Robinson, D.N., Binienda, W.K., Miti–Kavuma,M., "Creep and Creep Rupture of Strongly Reinforced Metallic Composites," NASA CR 185286, 1990.

60) Grobstein, T.L., "The Interface in Tungsten Fiber Reinforced Niobium Metal Matrix Composites," NASA TM 102122, 1989.

61) Robinson, D.N. and Duffy, S.F., "Continuum Deformation Theory for High Temperature Metallic Composites," J. Eng. Mech., ASCE, Vol. 116, No. 4, Apr. 1990, pp. 832–844

62) Arnold, S.M., "A Transversely Isotropic Thermoelastic Theory," NASA TM 101302, 1989.

63) Bartolotta, P., "Fatigue Life Prediction of an Intermetallic Matrix Composite at Elevated Temperature," NASA TM 104494, 1991.

64) Sines, G., "Behavior of Metals Under Complex Static and Alternating Stresses," Metal Fatigue, G. Sines and J.L. Waisman (eds.), Mc Graw Hill, 1959, pp. 145–169.

65) Crossland, B., "Effect of Large Hydrostatic Pressures on the Torsional Fatigue Strength of an Alloy Steel," Proceedings, International Conference on Fatigue of Metals, Institute of Mechanical Engineering, London, 1956, pg. 138.

66) Manson, S.S., "Interfaces between Fatigue, Creep and Fracture," Int. Jnl. of Fract. Mech., Vol 2, No 1, 1966, pp. 327–363.

Table I : The Leckie–Hayhurst Creep Damage Model

Multiaxial:

$$\frac{dD_c}{dt} = \left[\frac{\chi(\sigma^d_{ij})}{A_c}\right]^r (1-D_c)^{-k}$$

with

$$\chi(\sigma_{ij}) = \alpha_c\, J_0(\sigma_{ij}) + \beta_c\, \mathcal{A}_1(\sigma_{ij}) + (1-\alpha_c-\beta_c)\, \bar{J}_2(\sigma_{ij})$$

$$J_0(\sigma_{ij}) = \max_i \sigma_{ii} \quad ; \quad \mathcal{A}_1(\sigma_{ij}) = \sigma_{kk} \quad ; \quad \bar{J}_2(\sigma_{ij}) = \sqrt{\frac{3}{2} S_{ij} S_{ij}}$$

where

$$S_{ij} = \sigma_{ij} - \frac{\sigma_{kk}}{3} \delta_{ij}$$

$$\frac{d\sigma^d_{ij}}{dt} = \frac{\sigma_{ij}-\sigma^d_{ij}}{\tau}$$

and σ_{ij} is replaced by σ^d_{ij} in the creep model

A_c, r, k, α_c, β_c, and τ are material parameters, A_c and r are typically taken to be temperature dependent.

Uniaxial

$$\frac{dD_c}{dt} = \left[\frac{\sigma^d}{A_c}\right]^r (1-D_c)^{-k}$$

Table II : Fatigue Damage Models (ONERA NLCDM Multiaxial Form)

Model I :

$$dD_F = [1-(1-D_F)^{\beta+1}]^{\alpha} \left[\frac{\mathscr{A}_1}{M(\mathscr{A}_2)} \frac{}{(1-D_F)}\right]^{\beta} dN$$

where

$$\alpha = 1 - a \frac{<\mathscr{A}_1 - S_\ell(\mathscr{A}_2)>}{<\sigma_u - \mathscr{A}_3>}$$

$$M(\mathscr{A}_2) = M_0 (1-b \, \mathscr{A}_2)$$

$$S_\ell(\mathscr{A}_2) = S_{0\ell} (1-b' \, \mathscr{A}_2)$$

Model II :

Micro initiation :

$$N_i = \frac{C_0}{1+\left[\dfrac{\nu_0}{\nu}\right]^{\gamma}} \left[\frac{<\mathscr{A}_1 - S_i(\mathscr{A}_2)>}{<\sigma_u - \mathscr{A}_3>}\right]^{-\beta_i}$$

$$S_i(\mathscr{A}_2) = S_{0i} (1-b'' \, \mathscr{A}_2)$$

Micro propagation :

$$dD_F = [1-(1-D_F)^{\beta+1}]^{\alpha} \left[\frac{\mathscr{A}_1}{M(\mathscr{A}_2)} \frac{}{(1-D_F)}\right]^{\beta} \frac{<\mathscr{A}_1 - S_p(\mathscr{A}_2)>}{<\sigma_u - \mathscr{A}_3>} dN$$

$$\alpha = 1 - a$$

$$S_p(\mathscr{A}_2) = S_{0p} (1-b' \, \mathscr{A}_2)$$

Table II **(Conclusion)**

Model III :

$$dD_F = [1-(1-D_F)^{\beta+1}]^\alpha \; [\frac{\mathcal{A}_1}{M(\mathcal{A}_2)} - \frac{1}{(1-D_F)}]^\beta \; H(\mathcal{A}_1 - S_p(\mathcal{A}_2)) \; dN$$

where $\quad \alpha = 1 - a \; \dfrac{<\mathcal{A}_1 - S_\ell(\mathcal{A}_2)>}{<\sigma_u - \mathcal{A}_3>}$

$$M(\mathcal{A}_2) = M_0 \; (1 - b\mathcal{A}_2)$$

$$S_\ell(\mathcal{A}_2) = S_{0\ell} \; (1 - b'\mathcal{A}_2)$$

$$S_p(\mathcal{A}_2) = S_{0p} \; (1 - b'\mathcal{A}_2)$$

Note M_0, $S_{0\ell}$, S_{0i}, S_{0p}, a, b ,b' ,b" , β, γ and σ_u are material parameters with σ_u also taken to be temperature dependent.

For all three models :

$$\mathcal{A}_1 = \frac{1}{2} \; \max_{t_1} \; [\max_{t_2} \; (\bar{J}_2[\sigma_{ij}(t_1) - \sigma_{ij}(t_2)])] \qquad \text{maximum amplitude}$$

$$\mathcal{A}_2 = \frac{1}{2} \; \{\max_t \; \mathcal{J}_1(\sigma_{ij}(t)) + \min_t \; \mathcal{J}_1(\sigma_{ij}(t))\} \qquad \text{mean stress}$$

$$\mathcal{A}_3 = \max_t \; \bar{J}_2(\sigma_{ij}(t)) \qquad \text{maximum octhaedral stress}$$

where $\mathcal{J}_1$ and $\bar{J}_2$ are defined in table I.

Table III : ONERA Fatigue Damage Models in Uniaxial Form

Model I :

$$dD_F = [1-(1-D_F)^{\beta+1}]^\alpha \; [\frac{\sigma_m - \overline{\sigma}}{M(\overline{\sigma}) \; (1-D_F)}]^\beta \; dN$$

$$\alpha = 1 - a \; \frac{<\sigma_m - \sigma_\ell(\overline{\sigma})>}{<\sigma_u - \sigma_m>}$$

$$\sigma_\ell(\overline{\sigma}) = \sigma_\ell(0) + (1-b \; \sigma_\ell(0)) \; \overline{\sigma}$$

$$M(\overline{\sigma}) = M_0 \; (1-b \; \overline{\sigma})$$

Model II :

Micro initiation :

$$N_i = \frac{C_0}{1+\left[\frac{\nu_0}{\nu}\right]^\gamma} \left[\frac{<\sigma_m - \sigma_{\ell i}(\overline{\sigma})>}{<\sigma_u - \sigma_m>} \right]^{-\beta_i}$$

$$\sigma_{\ell i}(\overline{\sigma}) = \sigma_{\ell i}(0) + (1-b \; \sigma_{\ell i}(0)) \; \overline{\sigma}$$

Micro propagation :

$$dD_p = [1-(1-D_p)^{\beta+1}]^\alpha \; [\frac{\sigma_m - \overline{\sigma}}{M(\overline{\sigma}) \; (1-D_p)}]^\beta \; \frac{<\sigma_m - \sigma_{\ell p}(\overline{\sigma})>}{<\sigma_u - \sigma_m>} \; dN$$

$$\alpha = 1-a$$

$$M(\overline{\sigma}) = M_0 \; (1-b \; \overline{\sigma}))$$

$$\sigma_{\ell p} = \sigma_{\ell p}(0) + (1-b \; \sigma_{\ell p}(0)) \; \overline{\sigma}$$

where $\qquad N_F = N_i + N_p$

Table III (Conclusion)

Model III :

$$dD_F = [1-(1-D_F)^{\beta+1}]^{\alpha} \; [\frac{\sigma_m-\bar{\sigma}}{M(\bar{\sigma}) \; (1-D_F)}]^{\beta} \; H(\sigma_m-\sigma_{\ell p}(\bar{\sigma})) \; dN$$

$$\alpha = 1 - a \; \frac{<\sigma_m-\sigma_{\ell}(\bar{\sigma})>}{<\sigma_u-\sigma_m>}$$

$$\sigma_{\ell}(\bar{\sigma}) = \sigma_{\ell}(0)+(1-b \; \sigma_{\ell}(0)) \; \bar{\sigma}$$

$$M(\bar{\sigma}) = M_0 \; (1-b \; \bar{\sigma})$$

$$\sigma_{\ell p} = \sigma_{\ell p}(0)+(1-b \; \sigma_{\ell p}(0)) \; \bar{\sigma}$$

$$H(f) \begin{cases} = 1 \text{ if } f \geq 0 \\ = 0 \text{ if } f < 0 \end{cases}$$

where, in the three models M_0, $\sigma_{\ell}(0)$, $\sigma_{\ell i}(0)$, $\sigma_{\ell p}(0)$, b, a, β, γ, σ_u are defined as material properties.

·Table IV : Multiaxial Transversely Isotropic Fatigue Damage Models

Model I :

$$dD_F = [1-(1-D_F)^{\beta+1}]^\alpha \; [\frac{\hat{F}_m}{(1-D_F)}]^\beta \; dN$$

where

$$\alpha = 1 - a \; \frac{<\hat{F}_f \ell^{-1}>}{<1-\hat{F}_u>}$$

and

$$\sigma_{f\ell_L} = \sigma_{f\ell_L}(0) \; (1-3b' \; P)$$

$$M_L = M_{0_L} \; (1-3b \; P)$$

Model II :

Macro initiation

$$N_i = \frac{C_0}{1+\left[\frac{\nu_0}{\nu}\right]}^{-\gamma} \left[\frac{<\hat{F}_f \ell_i^{-1}>}{<1-\hat{F}_u>}\right]^{-\beta_i}$$

and

$$\sigma_{f\ell_L}i = \sigma_{f\ell_L}i(0) \; (1-3b'' \; P)$$

Macro propagation :

$$dD_p = \frac{\sigma_{f\ell_L P}}{\sigma_{u_L}} \; [1-(1-D_p)^{\beta+1}]^\alpha \; [\frac{\hat{F}_m}{(1-D_p)}]^\beta \; \frac{<\hat{F}_f \ell_p^{-1}>}{<1-\hat{F}_u>} \; dN$$

with

$$\alpha = 1-a$$

$$\sigma_{f\ell_L}p = \sigma_{f\ell_L}p(0) \; (1-3b' \; P)$$

$$M_L = M_{0_L} \; (1-3b \; P)$$

Table IV (Conclusion)

Model III :

$$dD_F = \sigma_{f\ell_L p} \; [1-(1-D_F)^{\beta+1}]^\alpha \; [\frac{\hat{F}_m}{(1-D_F)}]^\beta \; H(F_{f\ell p}-1) \; dN$$

with $\qquad \alpha = 1 - a \; \dfrac{<\hat{F}_{f\ell}-1>}{<1-\hat{F}_u>}$

$$\sigma_{f\ell_L} = \sigma_{f\ell_L}(0) \; (1-3b' \; P)$$

$$\sigma_{f\ell_L p} = \sigma_{f\ell_L p}(0) \; (1-3b' \; P)$$

$$M_L = M_{0_L} \; (1-3b \; P)$$

where a, b, b', b," β, γ, $\sigma_{f\ell_L}(0)$, $\sigma_{f\ell_L i}(0)$, $\sigma_{f\ell_L p}(0)$, σ_{u_L}, M_{0_L} are material coefficients with σ_{u_L} being taken to depend on temperature.

Note that :

$$\sigma_{Havg} = \frac{1}{2} \; \{\max_t \; (\sigma_{ii}(t))+\min_t \; (\sigma_{ii}(t))\} \qquad \text{mean hydrostatic stress}$$

$$\sigma_{Hmax} = \max_t \; (\sigma_{ii}(t)) \qquad \text{max hydrostatic stress}$$

$$P = \zeta \; \sigma_{Hmax}+(1-\zeta) \; \sigma_{Havg} \qquad \text{(combines the Sines and Crossland criteria)}$$

t – is time during a cycle

Table V : Baseline Dimensionless Parameters for Isotropic and Anisotropic Materials

Isotropic			Transversely Isotropic		
$\mathcal{R}$	=	0.25	$\mathcal{R}$	=	0.25
$\mathcal{M}$	=	4.5	$\mathcal{M}$	=	4.5
β	=	3.0	β	=	3.0
a	=	0.1	a	=	0.1
$\overline{S}$	=	0.0	$\overline{S}$	=	0.0
ω_m	=	1.0	ω_m	=	5.0
$\omega_{f\ell}$	=	1.0	$\omega_{f\ell}$	=	5.0
ω_u	=	1.0	ω_u	=	5.0
η_m	=	1.0	η_m	=	2.0
$\eta_{f\ell}$	=	1.0	$\eta_{f\ell}$	=	2.0
η_u	=	1.0	η_u	=	2.0

Figure 1.—Schematic of effective stress concept and equivalence in strain.

46
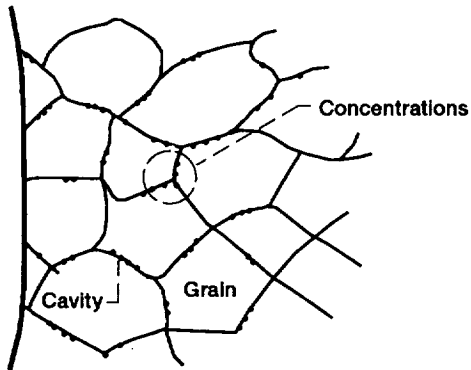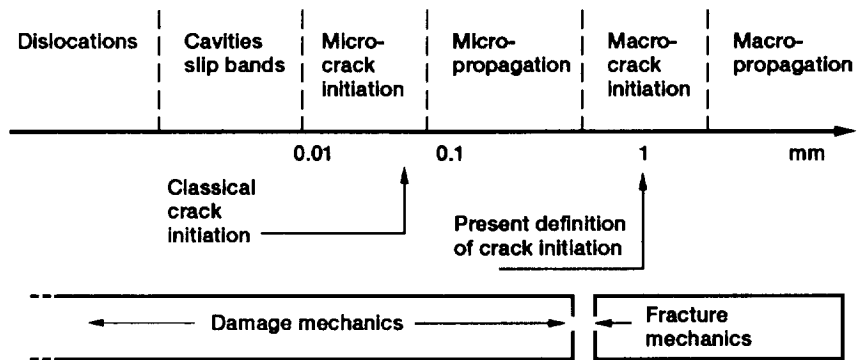
(a) Creep damage: coalescence of cavities and intergranular defects.
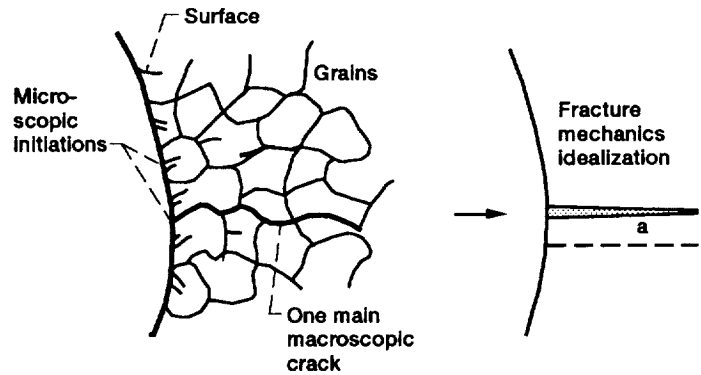
(b) Fatigue damage: nucleation of slip bands, microcracks and transgranular defects.
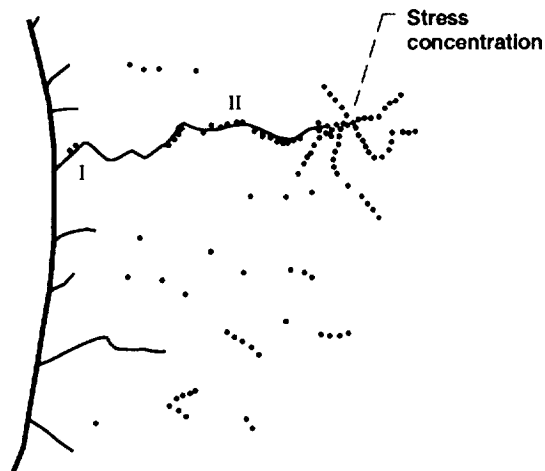
(c) Creep/fatigue damage: interaction of intergranular and transgranular defects.

Figure 2.—Schematic of different damage modes and the associated scale in a monolithic metal.
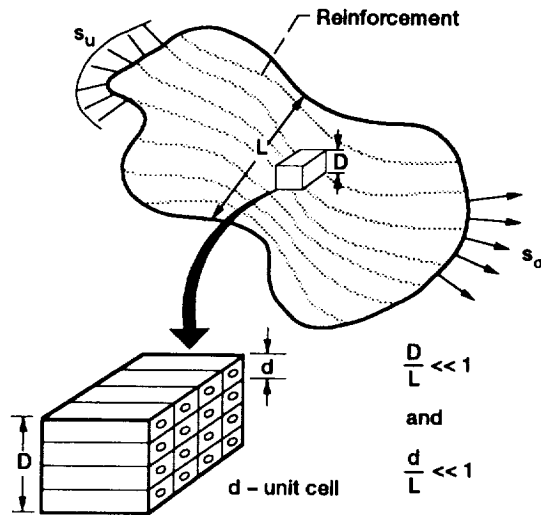
Figure 3.—Nonrigorous definition of representative volume element.

Micro crack propagation	Mesostructural crack initiation	Mesostructural crack propagation	Macro crack initiation	Macro crack propagation

0.1   1   mm

(a) Creep damage by way of intergranular void growth.

(b) Fatigue damage: initiation and propagation of transgranular defects.

(c) Creep-fatigue: interaction of intergranular and transgranular defects.
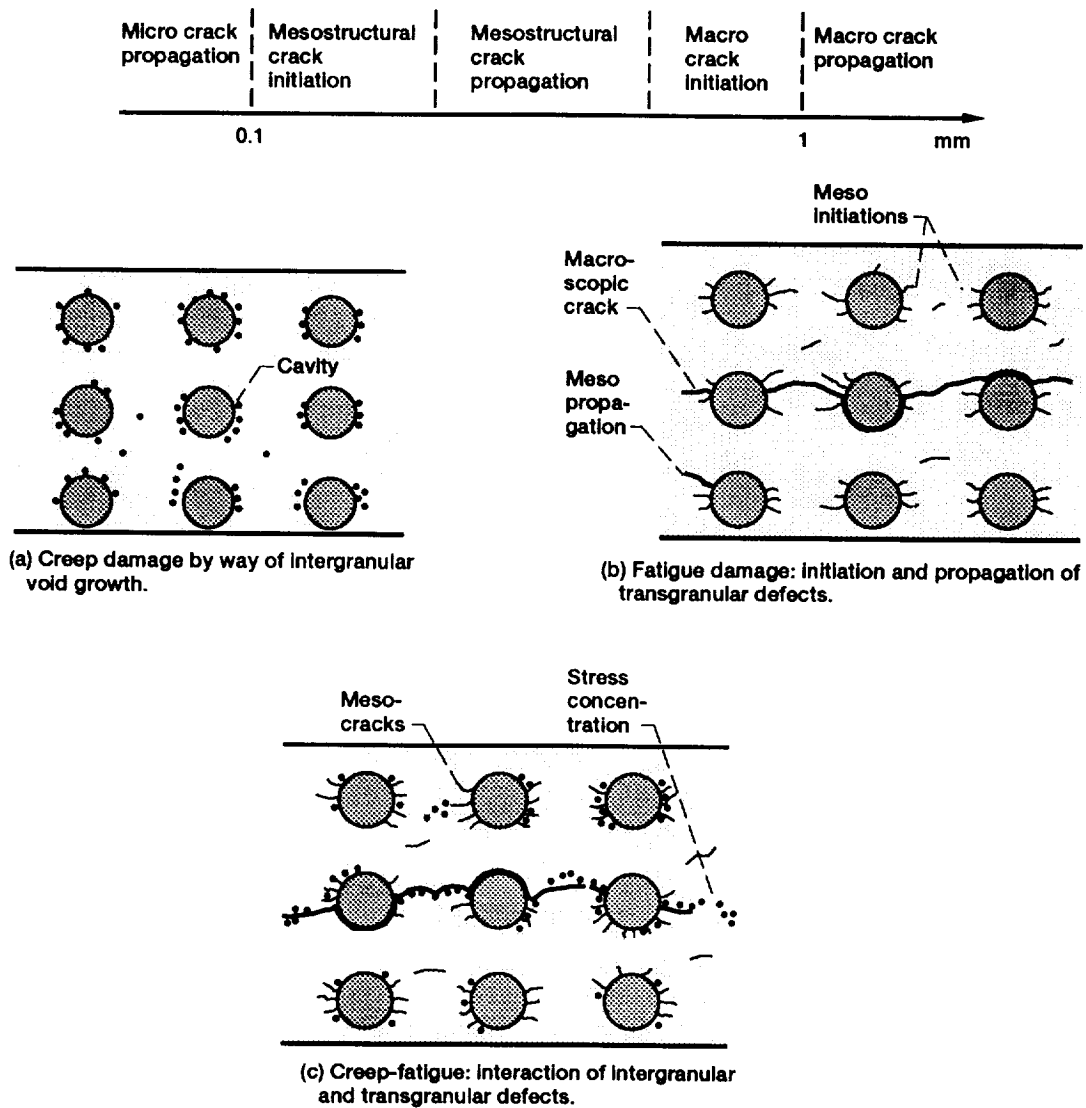
Figure 4.—Schematic of different damage modes and the associated scale in a metallic composite. Fibers on mesostructural scale are analogous to grain boundaries on microstructural scale.

48
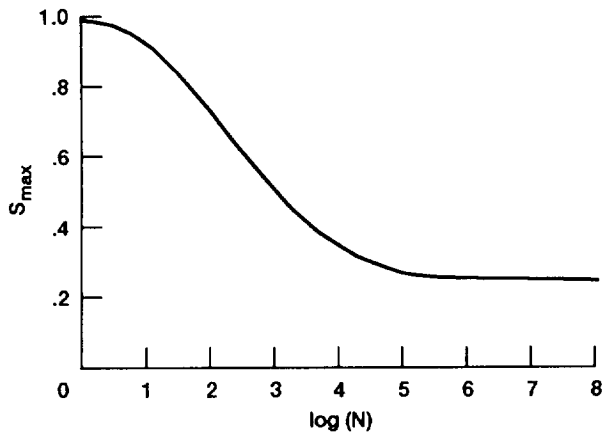
Figure 5.—Illustration of an S-N curve for the dimensionless isotropic baseline material parameters of Table V.
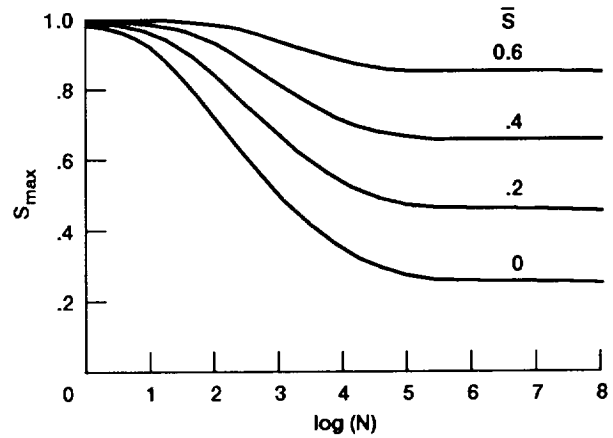
Figure 6.—Illustration of the effect on the S-N curve of varying the mean stress $\bar{S}$ = 0, 0.2, 0.4, 0.6, while holding all other parameters fixed.
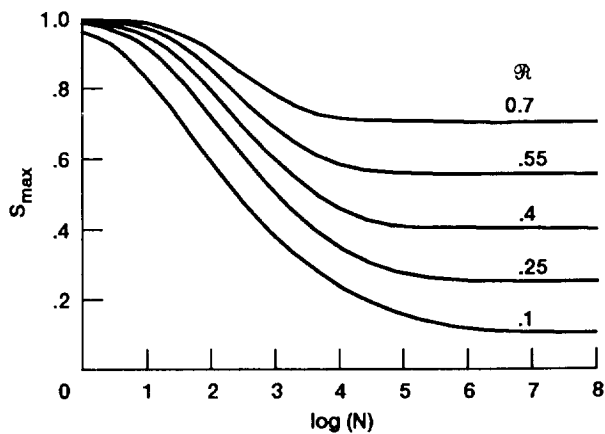
Figure 7.—Illustration of the effect on the S-N curve of varying the fatigue ratio $\mathcal{R}$ = 0.1, 0.25, 0.4, 0.55, 0.7, while holding all other parameters fixed.
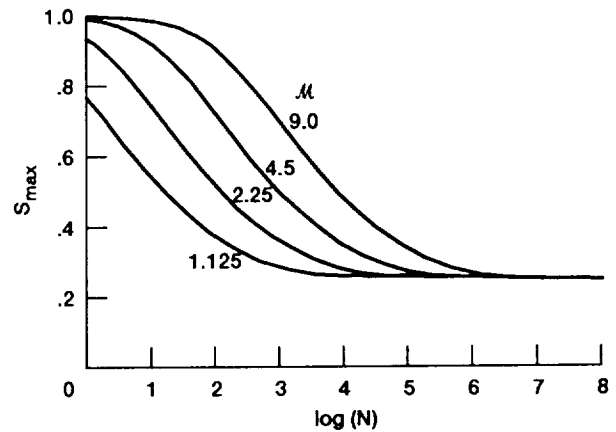
Figure 8.—Illustration of the effect on the S-N curve of varying the parameter $\mathcal{M}$ = 1.125, 2.25, 4.5, 9.0, while holding all other parameters fixed.
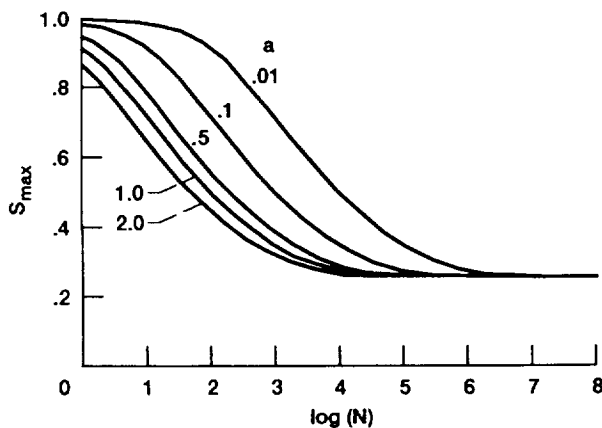
Figure 9.—Illustration of the effect on the S-N curve of varying the parameter a = 0.01, 0.1, 0.5, 1.0 and 2.0, while holding all other parameters fixed.
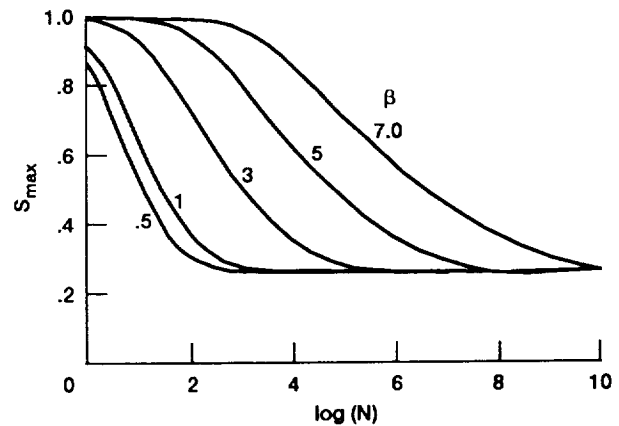
Figure 10.—Illustration of the effect on the S-N curve of varying the parameter β = 0.5, 1.0, 3.0, 5.0 and 7.0, while holding all other parameters fixed.
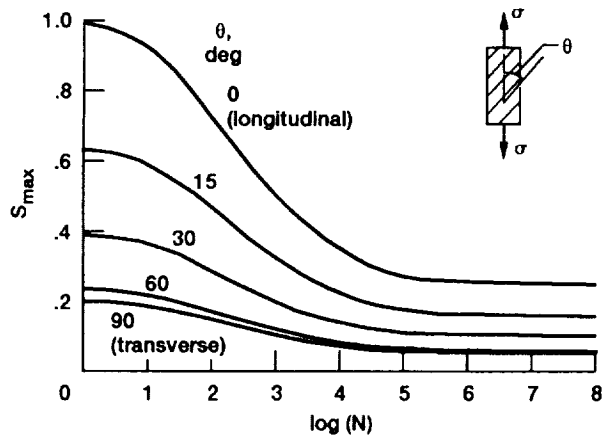
Figure 11.—Illustration of the degradation in load-life response with variation in fiber orientation, θ = 0, 15, 30, 60, and 90 degrees.
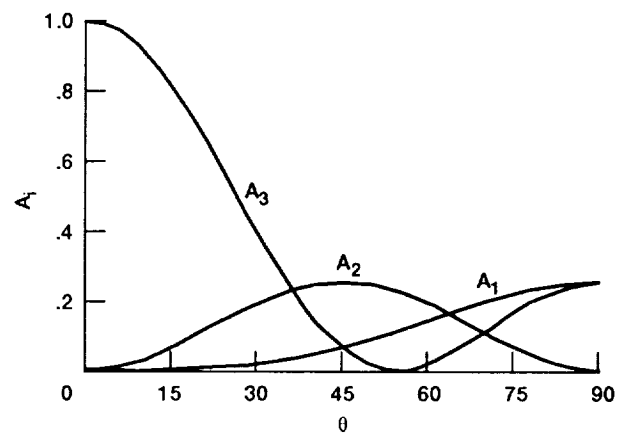
Figure 12.—The angle dependency of the longitudinal shear (A_1), transverse shear (A_2) and normal stress (A_3) components.
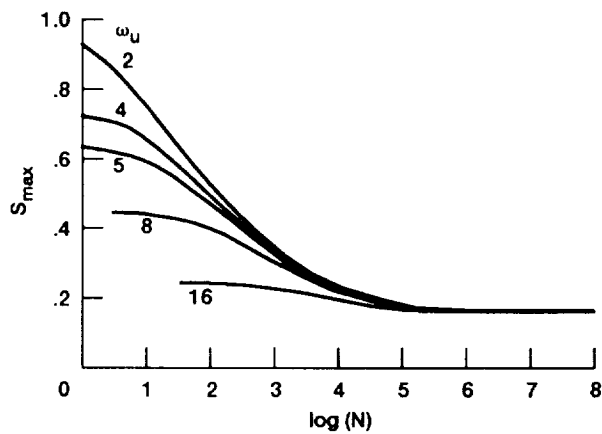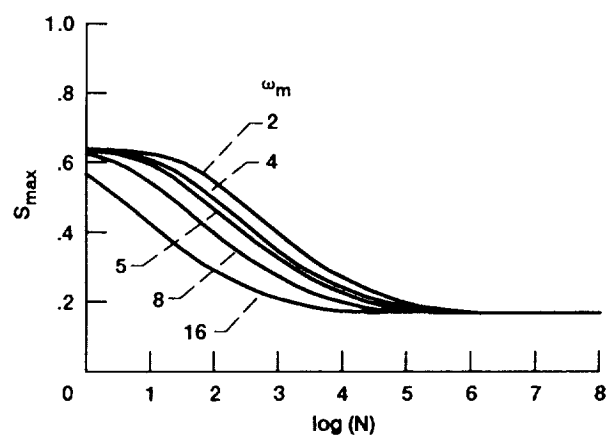

Figure 13.—Illustration of the effect on the S-N curve of varying the ratio ω_u = 2, 4, 5, 8, and 16, at an angle of 15 degrees, while holding all other parameters fixed at the baseline values.
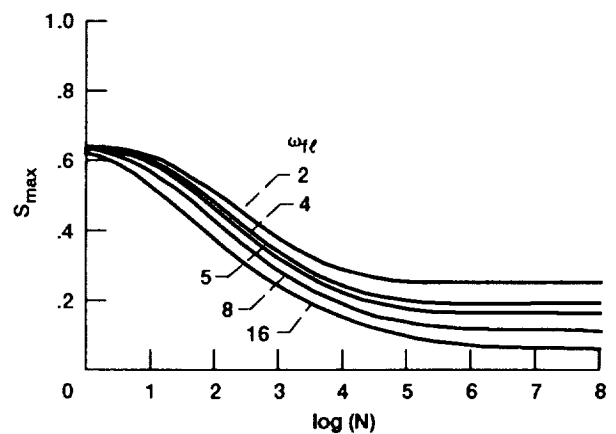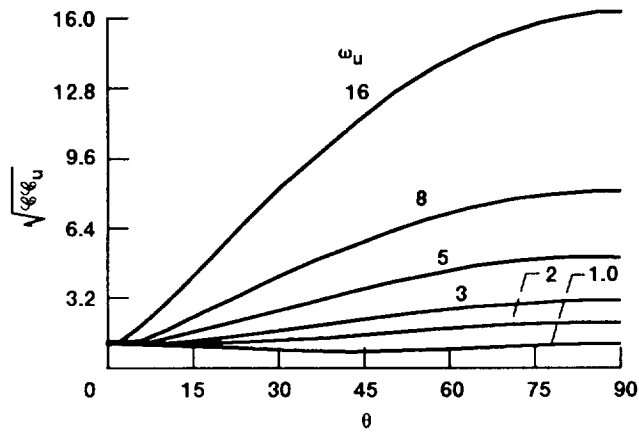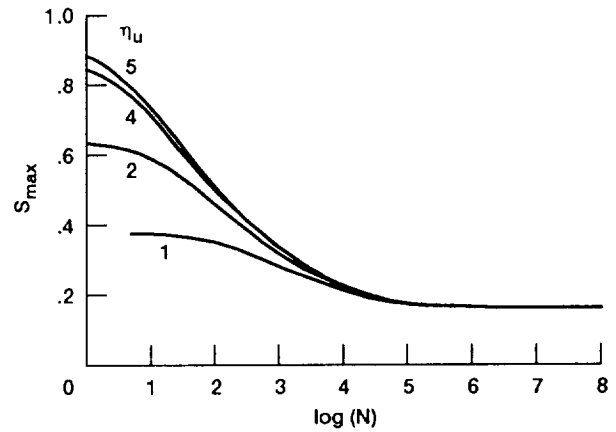

Figure 14.—Illustration of the effect on the S-N curve of varying the ratio $\omega_{f\ell}$ = 2, 4, 5, 8, and 16, at an angle of 15 degrees, while holding all other parameters fixed at the baseline values.
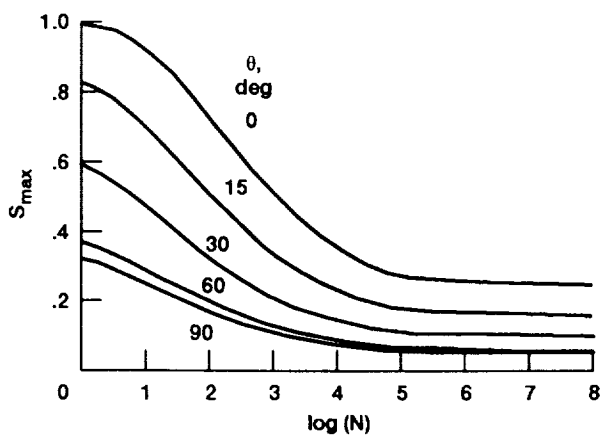
Figure 15.—Illustration of the effect on the S-N curve of varying the angle of fiber orientation θ = 0, 15, 30, 60, and 90 degrees with the ratio ω_u = 3 and all other parameters fixed at the baseline values.

Figure 16.—Illustration of the effect on the S-N curve of varying the ratio ω_m = 2, 4, 5, 8, and 16, at an angle of 15 degrees, while holding all other parameters fixed at the baseline values.

50

Figure 17.—Shows $\mathscr{C}\mathscr{C}_u$ versus angle of orientation θ, for varying ratios of ω_u, i.e., 1.0, 2.0, 3.0, 5.0, 8.0, and 16.0, when η_u = 2.0 and all other parameters are those in table V.

Figure 18.—Illustration of the effect on the S-N curve of varying the ratio η_u = 1, 2, 4, and 5, at an angle of 15 degrees, while holding all other parameters fixed at the baseline values.
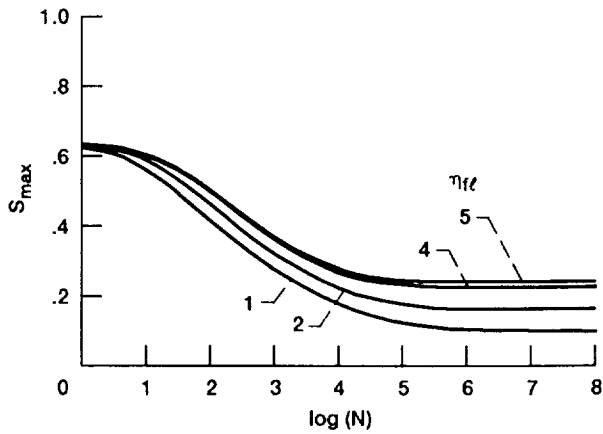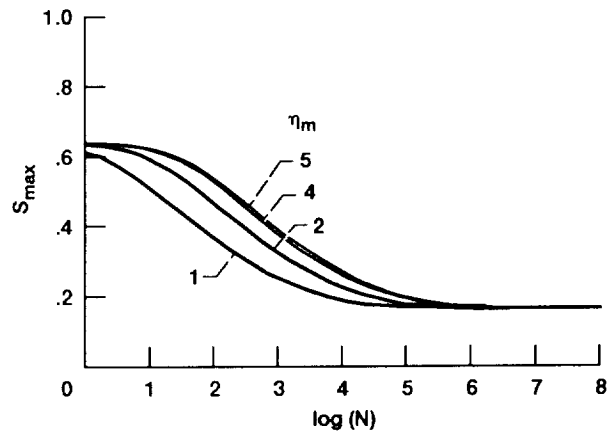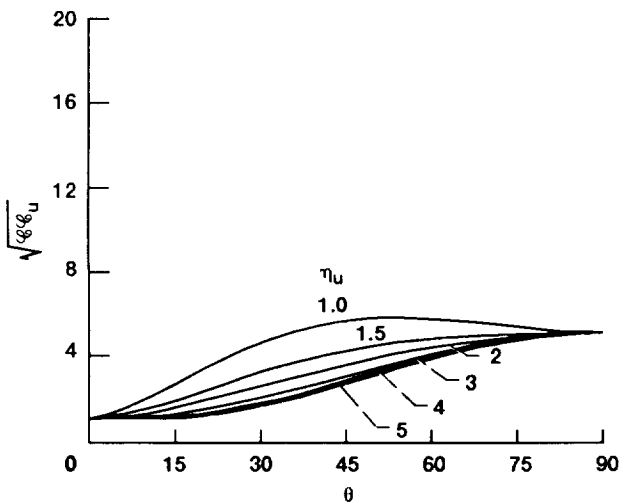

Figure 19.—Illustration of the effect on the S-N curve of varying the ratio $\eta_{f\ell}$ = 1, 2, 4, and 5, at an angle of 15 degrees, while holding all other parameters fixed at the baseline values.

Figure 20.—Illustration of the effect on the S-N curve of varying the ratio η_m = 1, 2, 4, and 5, at an angle of 15 degrees, while holding all other parameters fixed at the baseline values.

Figure 21.—Variation of $\mathscr{C}\mathscr{C}_u$ with angle of orientation θ, for varying ratios of η_u, i.e., 1.0, 1.5, 2.0, 3.0, 4.0, and 5.0, when ω_u = 5.0 and all other parameters are those in table V.
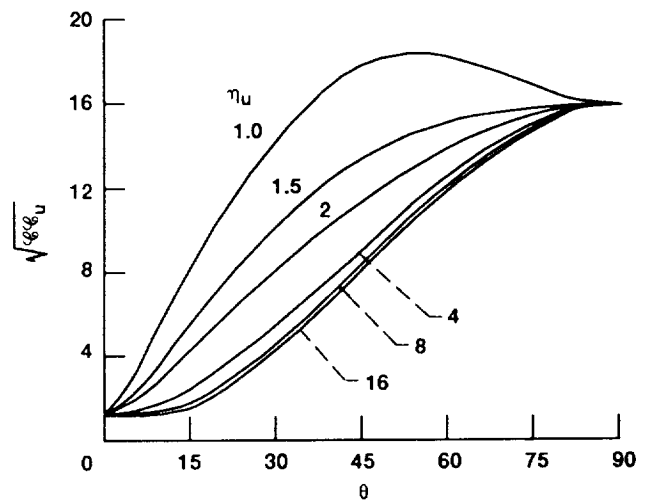

Figure 22.—Variation of $\mathscr{C}\mathscr{C}_u$ with angle of orientation θ, for varying ratios of η_u, i.e., 1.0, 1.5, 2.0, 4.0, 8.0, and 16.0, when ω_u = 16.0 and all other parameters are those in table V.
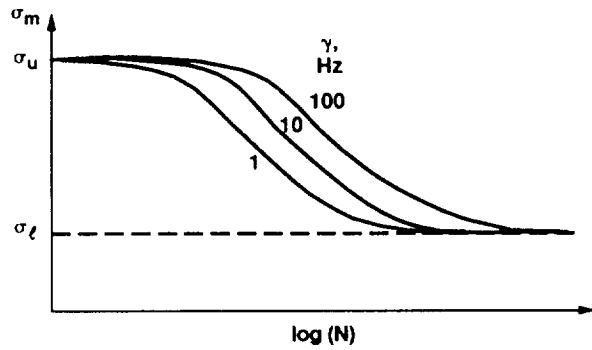
51

Figure 23.—Schematic of typical S-N curve for an isotropic metallic material, assumed to be known experimentally. Assuming $R = \sigma_{min}/\sigma_{max}$ and the mean stress $\bar{\sigma}$ to be held constant.
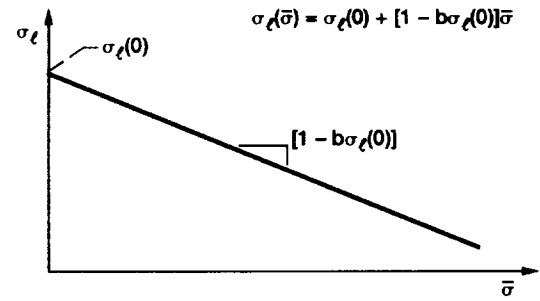

$$\sigma_\ell(\bar{\sigma}) = \sigma_\ell(0) + [1 - b\sigma_\ell(0)]\bar{\sigma}$$

Figure 24.—A plot of fatigue limit (σ_ℓ) versus mean stress $(\bar{\sigma})$, from which $\sigma_\ell(0)$ and b can be obtained.
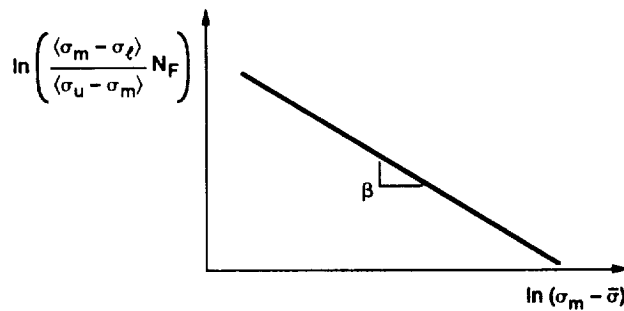

Figure 25.—A log-log plot of scaled cycles to failure versus stress amplitude is shown, from which the material parameter β can be found.
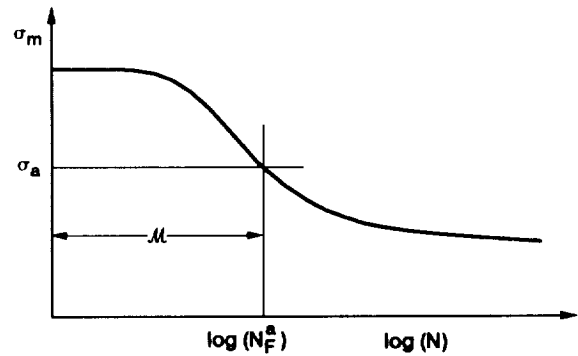

Figure 26.—A schematic of an S-N curve defining the meaning of the normalizing factor $\mathcal{M}$.

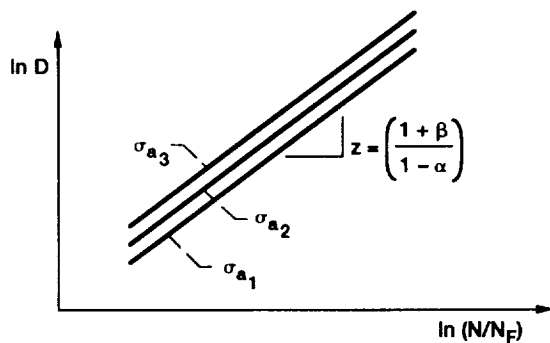$$z = \left(\frac{1+\beta}{1-\alpha}\right)$$

Figure 27.—A log-log plot of damage (D) versus remaining life (N/N_F) for various stress amplitudes.
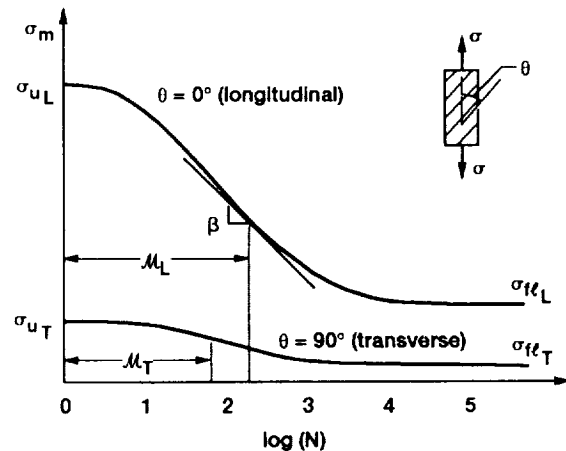

Figure 28.—A schematic depicting the expected S-N curves for a unidirectional metallic composite, when loaded longitudinally ($\theta = 0.0$) and transversely ($\theta = 90$).

52

REPORT DOCUMENTATION PAGE

Public reporting burden for this collection of information is estimated to average 1 hour per response, including the time for reviewing instructions, searching existing data sources, gathering and maintaining the data needed, and completing and reviewing the collection of information. Send comments regarding this burden estimate or any other aspect of this collection of information, including suggestions for reducing this burden, to Washington Headquarters Services, Directorate for information Operations and Reports, 1215 Jefferson Davis Highway, Suite 1204, Arlington, VA 22202-4302, and to the Office of Management and Budget, Paperwork Reduction Project (0704-0188), Washington, DC 20503.

1. AGENCY USE ONLY (Leave blank)	2. REPORT DATE	3. REPORT TYPE AND DATES COVERED
	November 1991	Technical Memorandum

4. TITLE AND SUBTITLE

Differential Continuum Damage Mechanics Models for Creep and Fatigue of Unidirectional Metal Matrix Composites

5. FUNDING NUMBERS

WU–510–01–50

6. AUTHOR(S)

S.M. Arnold and S. Kruch

7. PERFORMING ORGANIZATION NAME(S) AND ADDRESS(ES)

National Aeronautics and Space Administration
Lewis Research Center
Cleveland, Ohio 44135–3191

8. PERFORMING ORGANIZATION REPORT NUMBER

E–6629

9. SPONSORING/MONITORING AGENCY NAMES(S) AND ADDRESS(ES)

National Aeronautics and Space Administration
Washington, D.C. 20546–0001

10. SPONSORING/MONITORING AGENCY REPORT NUMBER

NASA TM–105213

11. SUPPLEMENTARY NOTES

S.M. Arnold, NASA Lewis Research Center; S. Kruch, Office National D'Etudes et de Recherches Aerospatiales, 92322 Chatillon, Chatillon, France. Responsible person, S.M. Arnold, (216) 433–3334.

12a. DISTRIBUTION/AVAILABILITY STATEMENT

Unclassified - Unlimited
Subject Category 39

12b. DISTRIBUTION CODE

13. ABSTRACT (Maximum 200 words)

Three multiaxial isothermal continuum damage mechanics models for creep, fatigue, and creep/fatigue interaction of a unidirectional metal matrix composite volume element are presented, only one of which will be discussed in depth. Each model is phenomenological and stress based, with varying degrees of complexity to accurately predict the initiation and propagation of intergranular and transgranular defects over a wide range of loading conditions. The development of these models is founded on the definition of an initially transversely isotropic fatigue limit surface, static fracture surface, normalized stress amplitude function and isochronous creep damage failure surface, from which both fatigue and creep damage evolutionary laws can be obtained. The anisotropy of each model is defined through physically meaningful invariants reflecting the local stress and material orientation. All three transversely isotropic models have been shown, when taken to their isotropic limit, to directly simplify to previously developed and validated creep and fatigue continuum damage theories. Results of a nondimensional parametric study illustrate i) the flexibility of the present formulation when attempting to characterize a large class of composite materials and ii) its ability to predict anticipated qualitative trends in the fatigue behavior of unidirectional metal matrix composites. Additionally, the potential for the inclusion of various micromechanical effects (e.g. fiber/matrix bond strength, fiber volume fraction, etc.), into the phenomenological anisotropic parameters is noted, as well as a detailed discussion regarding the necessary exploratory and characterization experiments needed to utilize the featured damage theories.

14. SUBJECT TERMS

Continuum mechanics; Cumulative damage; Fatigue life; Creep rupture; Metal matrix composites

15. NUMBER OF PAGES

54

16. PRICE CODE

A04

17. SECURITY CLASSIFICATION OF REPORT	18. SECURITY CLASSIFICATION OF THIS PAGE	19. SECURITY CLASSIFICATION OF ABSTRACT	20. LIMITATION OF ABSTRACT
Unclassified	Unclassified	Unclassified	

53 INTENTIONALLY BLANK

National Aeronautics and
Space Administration

Lewis Research Center
Cleveland, Ohio 44135

Official Business
Penalty for Private Use $300

NASA